

JOHNSON  
GRANT  
JN-39-CR  
253016  
67P.

A Final Report  
Entitled  
Payload Vibration Isolation in a Microgravity  
Environment

Grant No. NAS 9-17972

for the period  
6/1/88-12/31/89

Submitted by

Texas A&M Research Foundation  
College Station, Texas

to

National Aeronautics and Space Administration  
Lyndon B. Johnson Space Center  
Houston, Texas

Prepared by  
Richard M. Alexander  
Mechanical Engineering Department  
Texas A&M University  
College Station, Texas 77843-3123

January 15, 1990

(NASA-CR-186191) PAYLOAD VIBRATION  
ISOLATION IN A MICROGRAVITY ENVIRONMENT  
Final Report, 1 Jun. 1988 - 31 Dec. 1989  
(Texas A&M Univ.) 67 p CSCL 20K

N90-18744

Unclas  
63/39 0253016

## FOREWORD

This report was prepared in the Mechanical Engineering Department of Texas A&M University, College Station, TX 77843-3123. The work was performed in the Shock and Vibration Laboratory at Texas A&M under Contract NAS 9-17972 as part of the NASA Outreach program during the time period June 1988 to December 1989.

The concept of using air jets to control a vibration-sensitive payload in space originated with Dr. Carl H. Gerhold in 1986 while a NASA/ASEE Summer Fellow at NASA - Johnson Space Center. Dr. Gerhold, a Texas A&M University faculty member for 10 years until May 31, 1989, was a co-principal investigator on this project with Dr. Richard M. Alexander. Dr. Gerhold is currently with NASA - Langley Research Center in the Applied Acoustics Branch.

Clay B. Atwood and Joseph F. Cordera, graduate students supported by the project, developed the analytical model and experimental setup described in this report.

## ABSTRACT

Many in-space research experiments require the microgravity environment attainable near the center of mass of the Space Station. Disturbances to the structure surrounding an experiment may lead to vibration levels that will degrade the microgravity environment and undermine the experiment's validity. In-flight disturbances will include vibration transmission from nearby equipment and excitation from crew activity. Isolation of these vibration-sensitive experiments is imperative. This report summarizes the analytical and experimental work accomplished to develop a payload (experiment) isolation system for use in space. The isolation scheme discussed allows the payload to float freely within a prescribed boundary while being kept centered with forces generated by small jets of air. The vibration criterion employed in this project was a maximum payload acceleration of 10 micro-g's ( $9.81 \times 10^{-5} \text{m/s}^2$ ), independent of frequency. An experimental setup, composed of a cart supported by air bearings on a flat granite slab, was designed and constructed to simulate the microgravity environment in the horizontal plane. Experimental results demonstrate that the air jet control system can effectively manage payload oscillatory response. An analytical model was developed and verified by comparing predicted and measured payload response. The mathematical model, which includes payload dynamics, control logic, and air jet forces, is used to investigate payload response to disturbances likely to be present in the Space Station.

## TABLE of CONTENTS

FOREWORD	ii
ABSTRACT	iii
LIST OF FIGURES	v
LIST OF TABLES	vi
I. INTRODUCTION	1
II. PROGRAM OBJECTIVES	3
III. RELATIONSHIP to OTHER NASA EFFORTS	4
IV. METHOD of APPROACH and PRINCIPAL ASSUMPTIONS	
A. Experimental Setup	5
B. Control Methods	14
C. Pneumatic System Modeling	19
D. Analytical Model	29
V. BASIC DATA GENERATED and SIGNIFICANT RESULTS	36
VI. LIMITATIONS	57
VII. SUGGESTED ADDITIONAL EFFORT	58
VIII. CONCLUDING REMARKS	59
REFERENCES	60
DISTRIBUTION LIST	62

## LIST OF FIGURES

1. Air Jet Controller Setup	2
2. Isometric View of Experimental Setup	6
3. Top View of Experimental Setup	6
4. Dimensioned Experimental Setup	7
5. Payload Dimensions	7
6. Photograph of Experimental Setup	8
7. Controller Information Flow	9
8. Low Pass Filter and -5 Volt Offset Circuit	10
9. Control Algorithm Flowchart	17
10. Illustration of Displacement Control	18
11. Test Setup for Measuring Air Jet Forces	23
12. Comparison of Predicted and Measured Forces with Nozzle Diameter of 0.794 mm (1/32")	24
13. Section View of Small Nozzles	25
14. Section View of Large Nozzles	25
15. Comparison of Predicted and Measured Forces with Nozzle Diameter of 0.343 mm (0.0135")	26
16. Relationship of Air Jet Forces with Distance from the Jet	27
17. Illustration of Bernoulli Effects on Air Jet Forces	28
18. Single Degree-of-Freedom Model	34
19. Schematic of Test Setup for One-Dimensional Motion	34
20. Top View of Experiment and Coordinates Chosen	35
21. Relationship of Control Variables to Sensors	35
22. Experiment: Free Vibration, Y IC, Y Dir	38
23. Theory: Free Vibration, Y IC, Y Dir	38
24. Experiment: Free Vibration, Y IC, X Dir	39
25. Theory: Free Vibration, Y IC, X Dir	39
26. Experiment: Free Vibration, $\theta$ IC, $\theta$ Dir	40
27. Theory: Free Vibration, $\theta$ IC, $\theta$ Dir	40
28. Experiment: Displacement Control, X IC, X Dir	41
29. Theory: Displacement Control, X IC, X Dir	41
30. Experiment: Free Vibration, X IC, X Dir	42
31. Theory: Free Vibration, X IC, X Dir	42
32. Experiment: Displacement Control, $\theta$ IC, $\theta$ Dir	43
33. Theory: Displacement Control, $\theta$ IC, $\theta$ Dir	43
34. Experiment: Velocity Control, X IC, X Dir	44
35. Theory: Velocity Control, X IC, X Dir	44
36. Experiment: Velocity Control, $\theta$ IC, $\theta$ Dir	45
37. Theory: Velocity Control, $\theta$ IC, $\theta$ Dir	45
38. Experiment: Combinational Control, X IC, X Dir	46
39. Theory: Combinational Control, X IC, X Dir	46
40. Experiment: Combinational Control, $\theta$ IC, $\theta$ Dir	47
41. Theory: Combinational Control, $\theta$ IC, $\theta$ Dir	47
42. Harmonic Response Acceleration Magnitude Ratio	49
43. Payload Response to Harmonic Excitation with Combinational Control	52

44. Payload Response to Harmonic Excitation with Displacement Control	53
45. Uncontrolled Payload Response to a Single Half-sine Pulse	54
46. Payload Response to a Single Half-sine Pulse with Displacement Control	55
47. Payload Response to a Positive-Negative Pulse Pair with Displacement Control	56

---

#### LIST OF TABLES

1. Summary of Controller Parameters	16
-------------------------------------	----

## I. Introduction

Many microgravity experiments require a static gravitational environment of less than  $10^{-6}$  g. This type of environment can be obtained in space near the center of mass of the Space Station. Disturbances such as rotating equipment, crew push off, thruster fire and pumps near an experiment can cause vibrations that will exceed the  $10^{-6}$  g acceleration criterion (Gerhold and Rocha, 1988). Typical disturbances and associated accelerations likely to be encountered are:

1. Atmospheric drag ( $10^{-6}$  g)
2. Vibration of pumps and blowers of  $\pm 1$  mm at 10 Hz (0.4g)
3. Crew motion ( $10^{-4}$  g)
4. Occasional firing of control thrusters ( $10^{-4}$  g)  
(Garriot and DeBra, 1985).

A standard experiment (payload) will fit into racks attached to the Space Station structure. One way to eliminate vibration transmission from the structure to the payload is to allow the payload to float freely within the enclosure. Since usually there will be some type of utility lines, such as electricity or air, which connect an experiment to the structure, the payload cannot be perfectly "free-floating". These utility lines offer a medium through which vibration will be transmitted from the support structure to the experiment. Therefore the lines must be carefully designed so that the vibration transmitted through them does not cause the payload motion to exceed the acceleration criterion.

In order for this partially free-floating payload to be vibration isolated, active control is required to keep the payload centered within the enclosure during operation of the experiment. It is proposed to use small jets of air to push the payload back to the center as it drifts toward the side of the enclosure. To develop an isolation scheme, motion in three dimensions, or six degrees-of-freedom, must be considered. Since there are six degrees-of-freedom there must also be at least six control forces to have controllability of the payload. This project deals with the development of an isolation system for planar motion since the microgravity environment can be simulated on earth only in the horizontal plane. It is important to note that the controller to be designed is used only to center the payload, and not to control the vibration transmission.

### Previous Work

Prior work has been done to develop an experimental model to simulate the microgravity environment (Gerhold and Rocha, 1988; Park, 1987). A representative payload was supported on air bearings which floated on a flat granite slab, as shown in figure 1. Cantilever springs were employed to simulate the spring rate of the utility lines. Motion was detected with a linear variable differential transformer (LVDT) connected to the payload. This signal was used to determine when air jet forces, used to control

payload motion, should be applied. Frictional forces in the system dominated the dynamic response such that the effect of the air jet forces could not be clearly observed. Since even small forces play a significant role in the dynamics of the payload in a microgravity environment, subsequent work focused on reducing friction in the experimental model. The primary friction force, due to the LVDT arrangement, was reduced by replacing the LVDT with an ultrasonic transducer. Payload motion tests were performed in the one-dimensional case only (Park, 1987).

### Present Research

At the conclusion of Park's study, further work was needed to reduce friction in the experimental model to increase the effectiveness of the air jets in controlling payload dynamics. Coulomb friction at the point of contact between the cantilever springs and the payload was the primary target for reduction. Reduction of this friction was accomplished by introducing plastic Slinky® helical springs in place of the cantilever springs. This change drastically reduced the overall damping in the system. Since no straightforward, inexpensive way to measure micro-g response was available, a mathematical model was developed to predict payload acceleration response to various disturbances. Both the experimental and mathematical models were expanded to allow for two-dimensional motion.

Results from this study will give valuable insight into the design of a three-dimensional prototype isolation system.

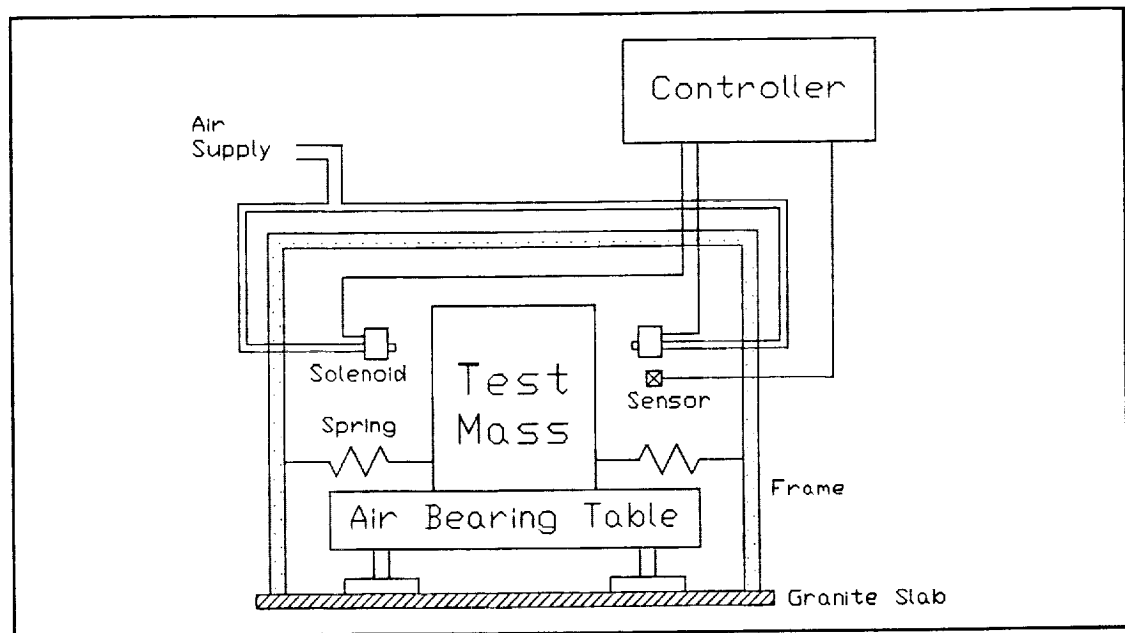


Figure 1 Air Jet Controller Setup

## II. PROGRAM OBJECTIVES

The objectives of this research study are to :

1. Devise a scheme to isolate vibrations transmitted from the Space Station structure to a vibration-sensitive experiment or payload;
2. Demonstrate this scheme analytically and experimentally in one and two-dimensional motion; the criterion for maximum payload acceleration is 10 micro-g's, independent of frequency.

### III. RELATIONSHIP to OTHER NASA EFFORTS

The work completed on this project was part of the NASA Outreach program, phase A feasibility study. The primary objective of the project was to develop a method to isolate vibration-sensitive, in-flight scientific experiments from structure-borne dynamic excitation. Many scientific experiments have flown and others will fly on space shuttle missions. The primary target for the technology developed during this project is the Space Station, where long-term vibration isolation of experiments will be required.

## IV. METHOD OF APPROACH and PRINCIPAL ASSUMPTIONS

### A. Experimental Setup

An experimental setup was designed to simulate a zero-g environment for general plane motion. This system consisted of a cart riding on air bearings, to represent the payload to be isolated, and helical springs to simulate utility connection stiffness. Instrumentation to monitor and control payload motion included ultrasonic sensors to measure displacements, air jets to generate control forces, a low-pass filter for noise reduction, a data acquisition board and a microcomputer.

#### Experiment

The air bearing cart was used to simulate an experimental payload (Figures 2-5) in the Space Station. The cart rides on three commercial air pads each measuring 15.2 cm x 15.2 cm arranged in an equilateral triangle beneath the cart. The center of mass of the cart is placed at the geometric center of the triangle to equalize the load on the pads. Air is fed to the pads through a small plastic hose from overhead. This vertical arrangement of the air hose minimizes the restoring force and damping caused by the hose. Although the air pads provided an extremely low friction simulation, an accurate value of system damping must be included in a theoretical model used to predict payload dynamic response.

Springs are used to simulate the stiffness of utility connections that may be needed for specific experiments. Soft springs are necessary to minimize the maximum payload acceleration level for a given vibration input. For this experiment a large plastic Slinky was found to possess an acceptably low spring rate. Attempts to measure the spring rate,  $K$ , were unsuccessful because the springs proved too soft to allow an accurate measurement of applied force for small displacements. A photograph of the experimental setup is shown in figure 6.

#### Controller

In previous work an analog controller was used for one-dimensional payload motion (Park, 1987). This type of controller proved inadequate for use in a two-dimensional controller. To provide flexibility in the development of control algorithms and straightforward expansion of the system to planar motion, a microcomputer with a data acquisition board was utilized. The computer was used to monitor incoming sensor measurements, store them and return appropriate control signals to the air jets. Figure 7 shows how the controller information flow was arranged.

To monitor payload displacement without contact ultrasonic sensors were employed. These sensors produce an analog dc voltage

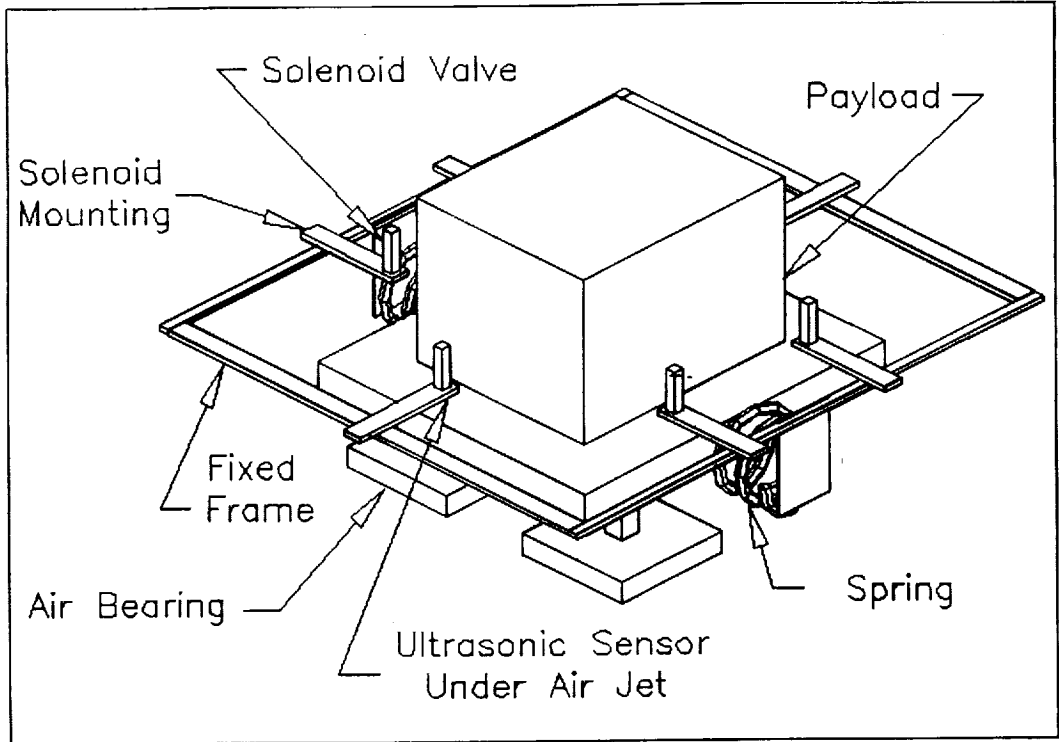


**Figure 2 Isometric View of Experimental Setup**

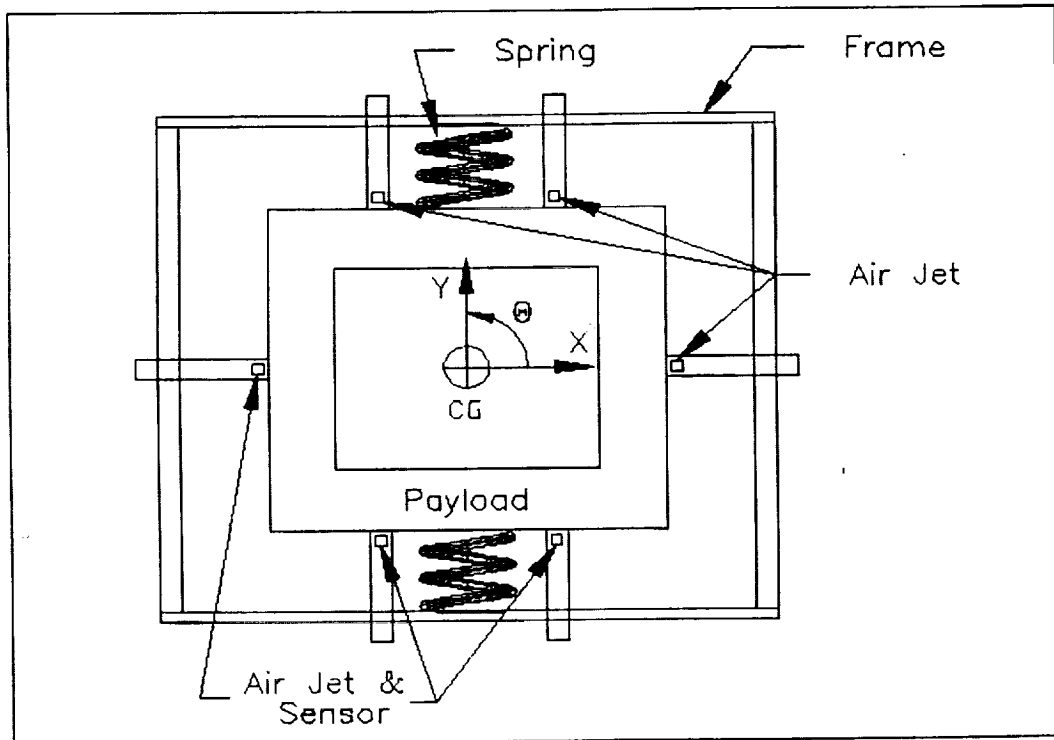


**Figure 3 Top View of Experimental Setup**

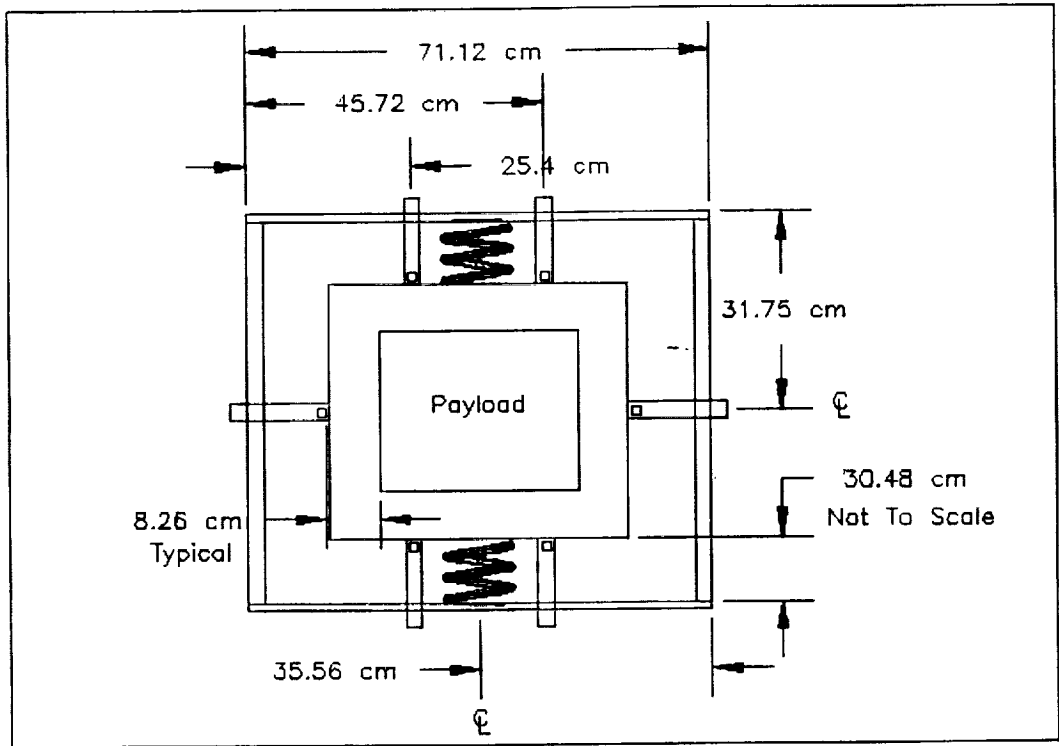


**Figure 4** Dimensioned Experimental Setup

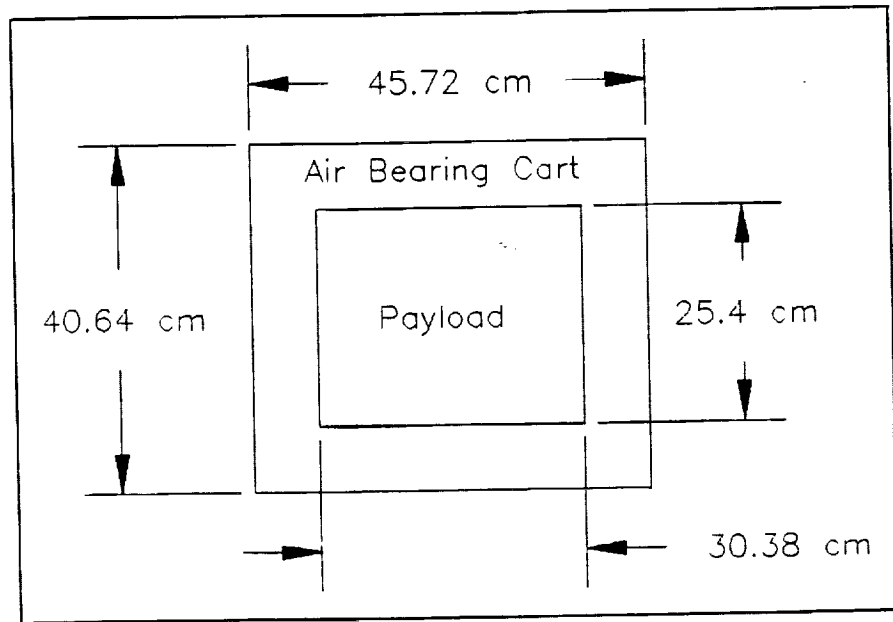


**Figure 5** Payload Dimensions

ORIGINAL PAGE  
BLACK AND WHITE PHOTOGRAPH

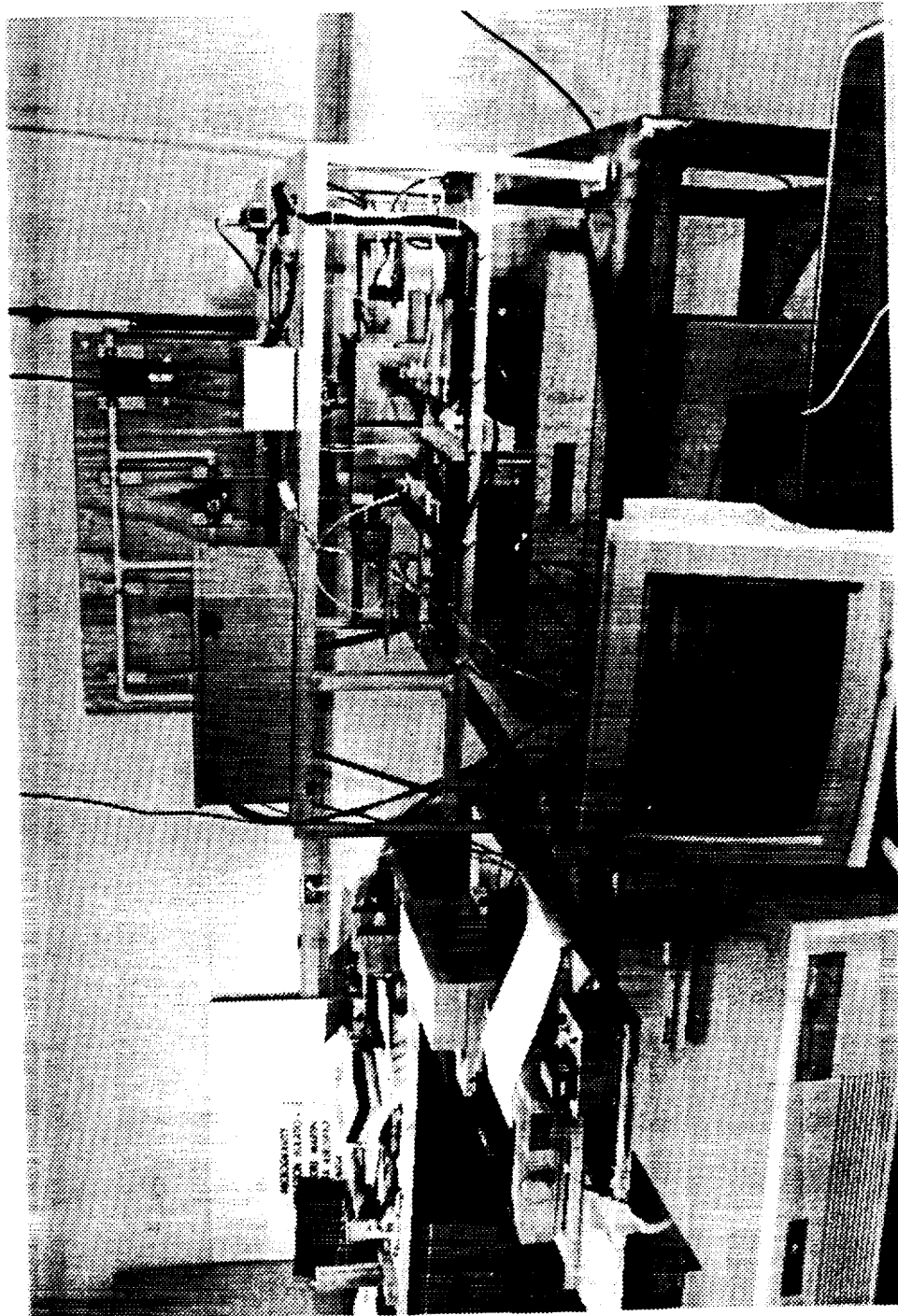


Figure 6 Photograph of Experimental Setup

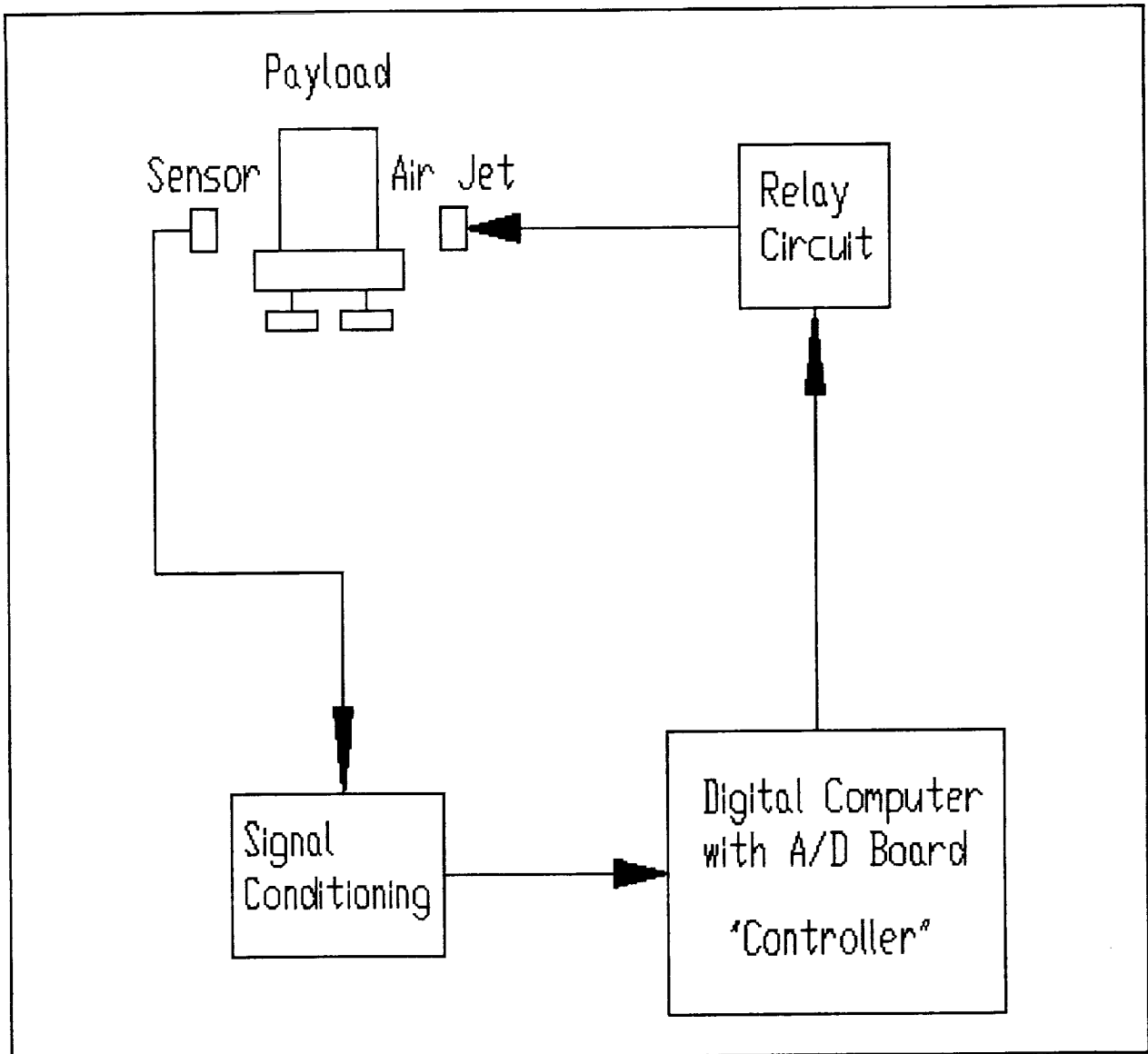


Figure 7 Controller Information Flow

given by the manufacturer as 0.79 mm (1/32"). Although the signal from the sensors could be read directly into the computer, noise from other equipment in the lab contaminated the signal. Also, the output of the sensor is 3.3-10 volts, while the A/D board's range is +/- 5 volts. A combination -5 volt offset and low-pass filter was implemented to alleviate these problems.

The low-pass filter was designed to remove noise above a given frequency. Response of the payload along with the frequency of the noise was considered in choosing the cutoff frequency. Since the frequency of the noise was 60 Hz and the highest natural frequency of the payload was approximately 0.0625 Hz, the cutoff frequency was chosen to be 1 Hz. A schematic of the filter and voltage offset

circuit is shown in figure 8. The -5 volt offset was obtained by summing the sensor input signal with -5 volts before filtering.

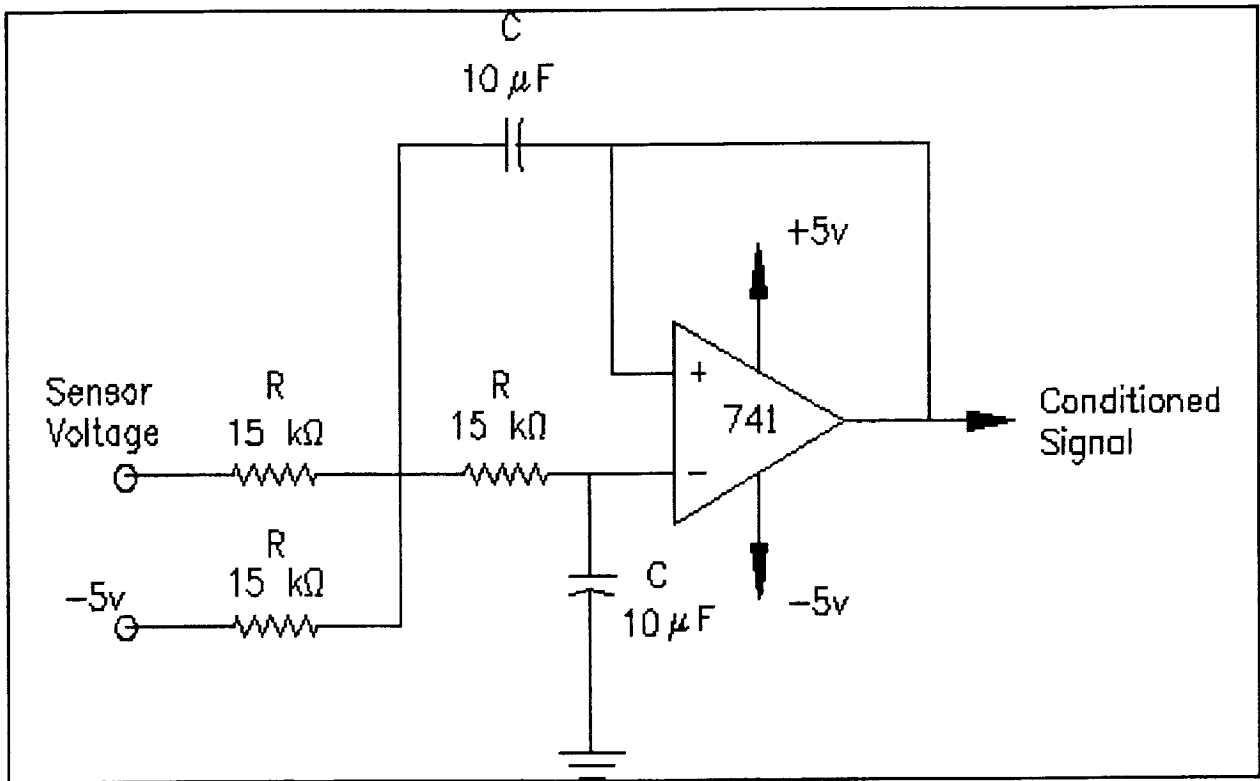


Figure 8 Low Pass Filter and -5 Volt Offset Circuit

This arrangement allowed the -5 volts to be filtered, then read into the computer and processed.

The computer used for the experiment was a Computer Access 386 with math coprocessor. In combination with the Data Translation DT2801A data acquisition board the computer system proved adequate for this application.

The DT2801A A/D board provided 16 channels of analog to digital conversion, 2 channels of digital to analog, and 16 bits of digital input/output. The analog to digital conversion was used to read the sensor voltage while the digital I/O was used to turn the air jets on and off via a relay circuit. The digital I/O produces a +5 volts when set high and 0 volts when set low. This type of control was implemented due to the number of jets and the fact that jets were only to be turned on or off. Once the measurements were read into the computer and processed, the digital control signal was output to the air jets. The computer output could not be used directly to fire the solenoids since they require AC voltage and more current than the computer can supply without damage. For this reason a relay circuit was designed to fire the solenoids while isolating the computer to avoid damage.

The relay circuit consists of six two-amp solid state relays which can be driven from a TTL output (computer). The relays used were Crydom D2W202F solid state relays. Relays functionally are switches to convert a low power DC voltage to a high power AC voltage. Once the relays switch on the AC voltage, a solenoid valve is opened which turns on the air to the nozzle providing the control force to the payload. The solenoids, manufactured by ASCO (Model U 8225 4), are designed to handle high pressure oil or air and proved to be unnecessarily large for this application. Smaller solenoids must be designed and implemented to minimize power requirements in the Space Station.

### **Air jet nozzles**

Air jet nozzles provide the forces required to control payload motion. Several different nozzle sizes were tested to determine jet force as a function of pressure. A detailed discussion of the air jets is given on p.19.

### **Software implementation**

Software was developed to acquire payload displacement data and use it to control payload motion, and to display real-time payload motion on the computer monitor during a test. The software was designed to provide a user-friendly environment with menu driven subroutines and error checking to prevent unwanted data loss. Error checking insures that the system has been calibrated and zeroed, with redundant inquiry before erasing data. Microsoft Compiled Quick Basic 4.5 was used to develop software. Although compilation provided better performance, it was not necessary for controller operation. The system also provides real-time data display, dead band and time step entry, and post digital filtering of the data.

### **Calibration and zeroing**

The manufacturer-provided calibration for the sensors could not be used due to the a signal conditioning incompatibility. A calibration subroutine was written to allow the user to calibrate each of the three sensors individually after signal conditioning to insure accurate results. Calibration is achieved by measuring the voltage output from the sensor at two known displacements. The sensitivity in volts per centimeter can then be calculated by assuming a linear voltage-position relationship. Sensor linearity was verified on several different occasions. It is recommended that the two points used for calibration be outside the range used for an actual experiment. Since sensors need not be calibrated each time the system was started, the program allows use of previous calibration data.

A zeroing subroutine was necessary since the control scheme was designed to use relative payload displacements measured from an initial equilibrium position. The zeroing subroutine provides the controller with the initial position of the payload. All displacements are then measured relative to that initial position. The system must be zeroed and calibrated before the program will allow tests to be run.

### Data conversion and display

Since the sensors do not measure the position of the payload mass center and its angular orientation  $(X, Y, \theta)$  directly, these values are calculated using relative sensor displacements from the zero position. By design the absolute zero position must be known in order to use relative displacements. A zeroing bar was used to secure the payload at the desired zero point. Assuming small rotations the following linearized equations relate payload position to sensor displacement (see figure 21, p.35.):

$$X = \delta_1 \cos^2 \theta + r_x (\cos \theta - \cos^2 \theta) - 0.5(\delta_2 + \delta_3) \theta \cos \theta$$

$$Y = 0.5(\delta_2 - \delta_3) + X\theta$$

$$\theta = (\delta_3 - \delta_2) / S$$

These equations reveal that X is dependent primarily on the left hand sensor while Y is based mostly on the bottom sensors. Rotation,  $\theta$ , however, is a function only of the bottom two sensors. This result is reasonable considering the alignment of the sensors with the axes and the small rotation angles. Although X, Y and  $\theta$  are not used in the controller scheme, they are calculated for real-time display.

Displaying the displacement variables in real time allows the user to determine whether a test is proceeding properly. This capability was valuable during controller development and final testing. The display subroutine allows the operator to view a time-history of the three variables by switching graphics pages using the cursor keys. A time-history of the variable provides information concerning the natural frequency, damping and coupling for that particular direction.

### Control algorithm

A control subroutine, the basis for the entire controller software, prompts the user to enter the velocity and displacement dead bands and the time step. The time step is the time between recorded data points and in no way affects the performance of the controller since the computer processes information at a sufficiently high sampling rate between recorded points. Velocity and displacement dead bands are centered about zero displacement and velocity such that when the displacement or velocity is inside these bands that portion of the controller is not activated. The

control scheme utilizes these dead bands to determine which jets should be fired. Details of the control schemes investigated and how the dead bands are used are discussed on p.14 .

## B. Control Methods

The following discussion addresses the types of control procedures considered in this study. Several ideas for regulating the force exerted by an air jet were appraised. One concept was to use some type of regulating device to vary the upstream pressure to a nozzle, hence varying the force exerted by the jet. Another technique considered was that of controlling the mass flow rate, and thus the jet force, with a variable diameter nozzle. After investigation, these ideas were abandoned in favor of an on-off force regulation method. The hardware for this type of control includes a solenoid valve to turn the air on or off and a constant diameter nozzle. This approach has limited flexibility since the only parameter that may be controlled is the on time of the solenoid. The on-off control scheme proved to be effective for this application.

In the experimental setup control system each ultrasonic transducer detects a displacement and sends a corresponding voltage to the A/D converter. Before the A/D converter receives the signal it is conditioned through an analog low-pass filter with a cutoff frequency of 1 Hz. The computer receives the digital signal from the A/D converter and differentiates it to obtain velocity. Usually differentiating a signal is not a wise practice due to noise in the system and the time lag involved, but the sampling rate here is high enough that the time lag is negligible and the filter removes most of the high frequency noise. However, some noise remained in the system after filtering. This noise in the displacement signal was amplified by the differentiation process. When the displacement and velocity values were near zero, the noise caused the signal to fluctuate between positive and negative. This fluctuation caused the solenoid valves to turn on and off rapidly, causing what was termed "chatter". To diminish this chatter, dead bands were placed in the control routine for both displacement and velocity. The velocity dead band used was 0.1 cm/sec and the displacement dead band was 0.5 mm. These values were determined by trial and error until the chatter was minimized and the damping produced by the air jet forces was not highly affected. From the velocity and displacement signals the control system determines which jets must be fired.

### Position control

Since the primary function of the control system is to keep the payload centered within a prescribed boundary, the most obvious type of control is to fire the jets in the direction to oppose the payload displacement as it moves off center. However, it was found experimentally that the payload motion tended to limit cycle with this control scheme. This phenomenon can be explained from the

work-energy relationship  $dE = F \cdot ds$ . As the payload drifts away from the center position, energy is dissipated because the jet force opposes the velocity; the dot product is negative. However, when the payload starts to drift back toward the center, the force continues to be applied in the same direction. This adds energy back into the system since the force and the velocity are in the same direction. If damping other than that due to the jets is neglected the system would limit cycle because the energy removed by the jets is immediately replaced. This control method, termed position control, is unsatisfactory; the discussion included here is for background information only.

### **General theory of schemes implemented**

Although each type of control scheme has its own particular characteristics, all controllers were designed to dissipate payload energy when activated, thus ensuring unconditional stability. This was achieved by only firing the control jets to oppose the velocity of the payload. Figure 9 is a flowchart of the controllers investigated.

### **Displacement control**

The first type of control thoroughly investigated was given the name displacement control since it is based on the position of the payload. For displacement control, the velocity dead band is set to a large number (10 cm/s) such that the payload motion will never exceed this threshold. A large velocity dead band will in effect remove the velocity portion (see figure 9) of the controller and allow the displacement dead band to be the only element used to fire the jet pair associated with each sensor. Displacement control will fire the positive jet when displacement is less than the negative dead band and the velocity is also less than zero and vice versa for the negative jet (figure 10). Although the velocity portion of the controller has been removed, the displacement controller requires the sign of the velocity to be checked to insure energy dissipation. Early tests run without the velocity dependence showed the system to be marginally stable. The dead band was needed due to noise in the displacement sensor signal.

The expected advantages of displacement control include the ability to completely damp payload oscillations such that the maximum payload acceleration meets the criterion and the controller has a low power consumption. The disadvantage is that this controller requires a longer time to damp the system. This leads to the next type of control, velocity control.

### **Velocity control**

Velocity control is similar to displacement control, but instead of basing control on the displacement of the payload, the velocity, as the name suggests, is used to fire the jet pairs. This type of controller is realized by setting the displacement dead

band to a large number (10 cm) and only allowing the velocity dead band to affect the control decision (again, refer to figure 9). By doing this the jets will always fire to oppose the velocity as long as it is greater than the threshold. Control is completely independent of the displacement. This type of control is expected to damp the payload motion more rapidly than with displacement control, but the system may continue to oscillate within the velocity dead band with an unacceptably high acceleration. Only the inherent system damping will remove energy from the payload motion once it is within the velocity dead band. Also, the payload may stop at a position other than the original zero point; thus the controller would not satisfy the criterion of centering the payload. These conditions lead to the final controller investigated, combinational control.

### Combinational control

Combinational control provides the advantages of the other two controllers by combining their logic. For this controller both the velocity and displacement dead bands are used for the control decision. By adjusting the two dead bands the effect of the two types of control can be varied to provide a high damping rate along with complete damping of the oscillation. This type of control was targeted as the controller of choice.

Table 1 summarizes the parameters of each controller.

Controller	Velocity Dead Band (cm/s)	Displacement Dead Band (cm)	Comments
Free Vibration	>10	>10	Jets are never fired
Displacement	>10	0.05	Jets fire when displ. & velocity have the same sign.
Velocity	0.1	>10	Jets fire to oppose velocity
Combinational	0.1	0.05	Combines the other controllers

Table 1 Summary of Controller Parameters

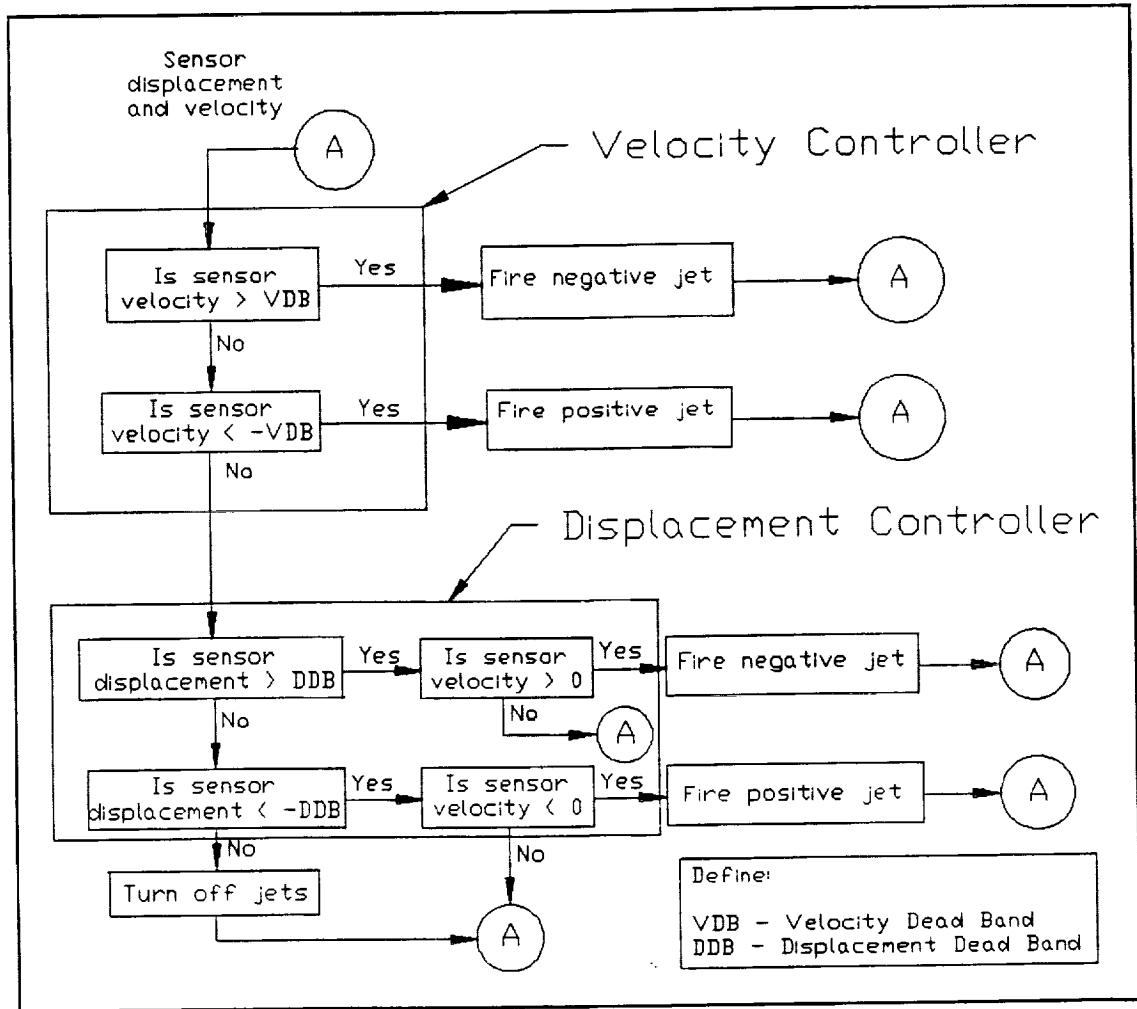
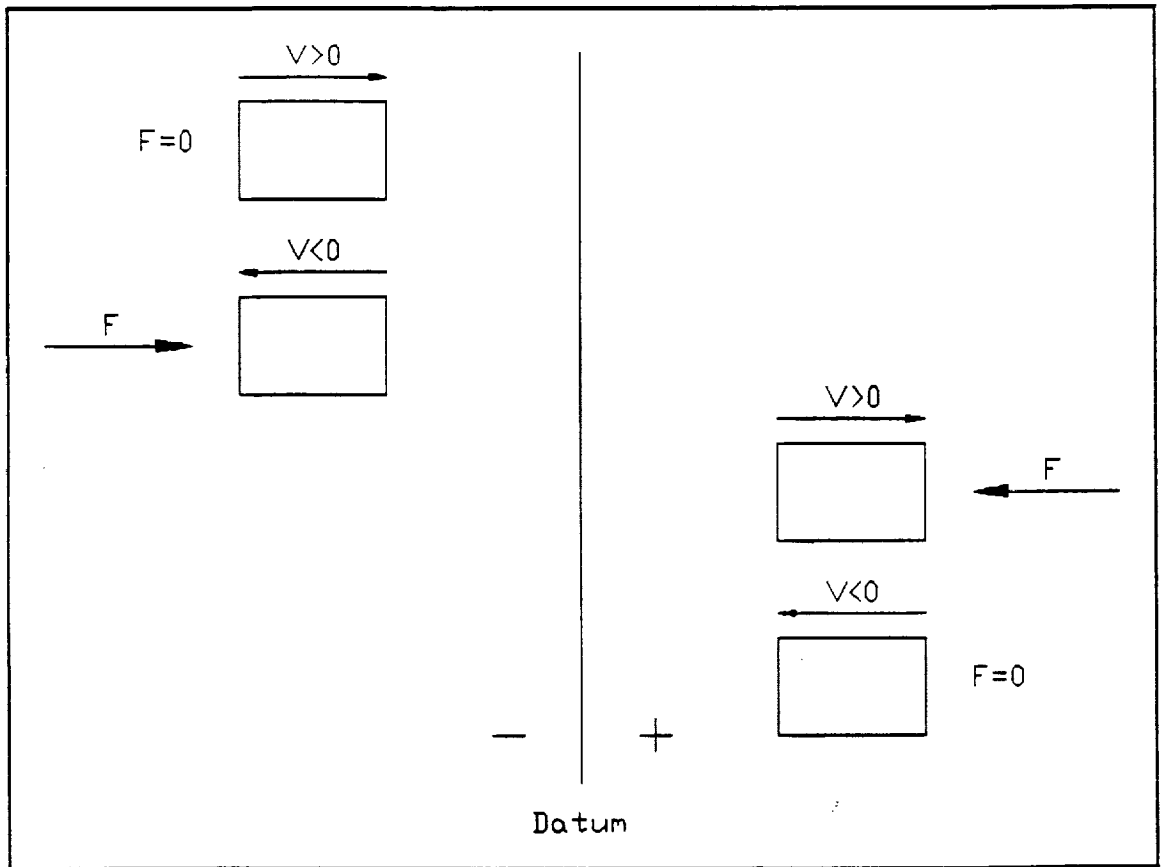


Figure 9 Control Algorithm Flowchart



**Figure 10** Illustration of Displacement Control

### C. Pneumatic System Modeling

We now discuss the mathematical model of the forces created by the air jets. Some of the considerations in developing the model were the transient response of the pneumatic system, the variation of jet force with distance from the jet nozzle, and the relationship of jet force with upstream pressure.

#### Transient response

The primary concerns with jet force transient response were overshoot and speed of response. If the jet force has a significant overshoot it must be considered in the design of an isolation system. A momentary peak force exerted on the payload may cause its acceleration to exceed the acceleration criterion and disrupt the scientific experiment in the Space Station. Also the transient response of the jet force must be included in the entire system analytical model. To investigate these concerns, an air jet of 0.79 mm (1/32") diameter with an upstream pressure of 34.5 kPa (5 psi) was fired into a capacitance microphone. From a time-history of the response there was found to be no detectable overshoot, and the transient response was complete in less than 6 ms. With these results it was concluded that the jet force could be modeled as a step function.

#### Force-pressure relationship

A relationship between pressure and jet force was developed by assuming isentropic flow. The pressure ratio is defined as the entrance pressure divided by the exit pressure. The relationship between pressure ratio and exit Mach number,  $M_e$ , is given by

$$\frac{P_o}{P_e} = \left[ 1 + \frac{k-1}{2} M_e^2 \right]^{k/(k-1)}$$

where  $k$  is the ratio of specific heats,  $C_p/C_v$ . Since air is the fluid,  $k=1.4$ . Rearranging the equation and solving for Mach number gives

$$M_e = \left[ \left[ \left( \frac{P_o}{P_e} \right)^{(k-1)/k} - 1 \right] \frac{2}{k-1} \right]^{1/2}$$

The velocity can be found from

$$V_e = M_e c_e,$$

where  $c_e$  is the speed of sound at the exit conditions, determined

from

$$c_e = \sqrt{kRT_e} ,$$

where R is the gas constant and  $T_e$  is the exit temperature.

The exit temperature is given by

$$T_e = \frac{T_o}{1 + \frac{k-1}{2} M_e^2}$$

where  $T_o$  is the upstream temperature. Solving these equations for exit velocity gives

$$V_e^2 = \left[ \frac{kRT_o}{k-1} \right] \left[ 1 - \left( \frac{P_e}{P_o} \right)^{(k-1)/k} \right]$$

The force from the jet is found from,

$$F = \dot{m} V_e$$

where mass flow rate,  $\dot{m}$ , is

$$\dot{m} = \rho_e M_e c_e A_e$$

and  $\rho_e$  is the density of the fluid

$$\rho_e = P_e / RT_e$$

Solving for the force,

$$F = \rho_e A_e \left[ \frac{kRT_o}{k-1} \right] \left[ 1 - \left( \frac{P_e}{P_o} \right)^{(k-1)/k} \right]$$

Since the vena contracta, or flow area through an orifice, is generally smaller than the exit area, an area correction factor,  $C_A$ , is incorporated. There are also energy losses which cause the exit velocity to be slightly lower than expected. A velocity correction factor,  $C_v$ , is included to account for this energy loss. The force equation becomes

$$F = C_A C_v^2 \rho_e A_e \left[ \frac{kRT_o}{k-1} \right] \left[ 1 - \left( \frac{P_e}{P_o} \right)^{(k-1)/k} \right]$$

To verify the mathematical model, air jet forces for several nozzle diameters were measured using a Metler scale (figure 11). The distance between the air jet and the scale plate was 25.4 mm (1.0"). After determining that there was a significant pressure loss across the solenoid valve, the pressure was measured between the valve and the nozzle. Using this pressure as the upstream pressure, the theoretical force was calculated and compared with measured values. Figure 12 shows a comparison for a nozzle diameter of 0.79 mm (1/32") with  $C_A = 1$  and  $C_V = 1$ ; the theory closely predicts actual jet forces for this jet size. Theoretical and measured forces also compared well for nozzle diameters of 0.597 mm (0.0235") and 1.016 mm (0.04").

However, the theory does not predict the force produced by several nozzle diameters tested as well as it did for the diameters listed above. The measured force deviates from the predicted force for nozzle diameters of 0.343 mm (0.0135"), 1.588 mm (1/16"), 2.381 mm (3/32"), and 3.175 mm (1/8"). Theory predicts a higher force than is actually measured. Reasons for this deviation are as follows. The nozzles with diameters of 0.343 (0.0135"), 0.597 mm (0.0235"), 0.794 mm (1/32"), 1.016 mm (0.04"), were drilled as shown in figure 13. The larger diameter bore was drilled the majority of the length, but a smaller diameter hole was drilled at the tip of the nozzle, which is the major restriction of air flow. It can be seen that there is a conical shape at the tip from the chamfer of the drill bit. This geometry allows the fluid to converge more slowly than would be observed in a sharp-edged orifice, reducing the energy loss. Since the fluid converges more slowly, the area of the vena contracta approaches the same magnitude as the nozzle diameter. However, the larger diameter nozzles of 1.588 mm (1/16"), 2.381 mm (3/32"), and 3.175 mm (1/8") were drilled through completely with the desired diameter drill bit (figure 14). The restriction is now at the entrance of the nozzle, not at the exit as with the smaller diameter nozzles. This restriction produces flow similar to that through a sharp-edged orifice. This type of flow causes large energy losses, decreasing  $C_V$ , and reduces the vena contracta, decreasing  $C_A$ .

The energy losses in the 0.343 mm (0.0135") diameter jet can be explained by discussing the boundary layer along the nozzle wall. As a fluid travels through a passage, its velocity profile is similar to a Gaussian distribution (Gerhold and Rocha, 1988). If the passage diameter is small, the boundary layer has a significant effect on the mean velocity of the fluid. Figure 15 shows predicted and measured values for a jet diameter of 0.343 mm (0.0135") with both correction factors set to 1.0. The opening is small enough that the boundary layer converges to restrict the flow. Since the actual forces are slightly lower than those predicted, the measured forces were used in the analytical model.

A relationship between the force of the air jet and the distance from the nozzle was needed to complete the pneumatic system model. The experimental setup shown in figure 11 was used to determine this relationship. The jet was arranged so that the air would impinge on the Metler scale. This type of scale was used

because little deflection is produced when a force is applied. The distance between the scale and the nozzle was varied and the force was recorded. Figure 16 shows the results for several pressures. It can be seen that the force is essentially constant for distances greater than 6.35 mm (1/4"). This constant force comes from the air entrainment as the velocity decreases (Gilbride, 1987). It is interesting to see that, if the distance becomes too small, the jet actually has an opposite force than is desired (figure 17). This phenomenon can be explained from Bernoulli's equation, which states that, neglecting gravitational effects, the pressure decreases as the velocity increases. At small distances the air strikes the plate but still has enough momentum that it travels along the surface of the plate. This velocity of the fluid causes the pressure to decrease on the surface of the plate, which in turn creates a negative force. However, if the distance is great enough, the velocity of the fluid traveling over the plate surface can be neglected and the force remains constant. From this information, the jets were placed in the experimental setup such that at the nozzle to payload distance was always greater than 12.7 mm (1/2").

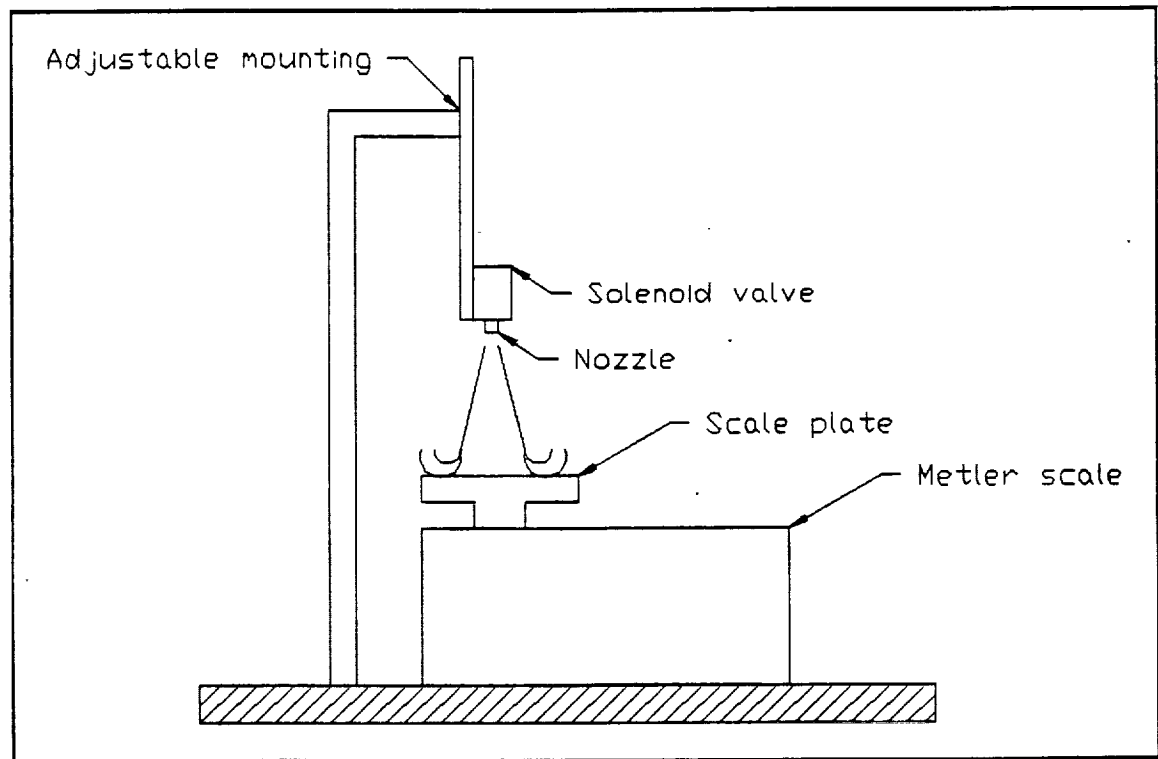


Figure 11 Test Setup for Measuring Air Jet Forces

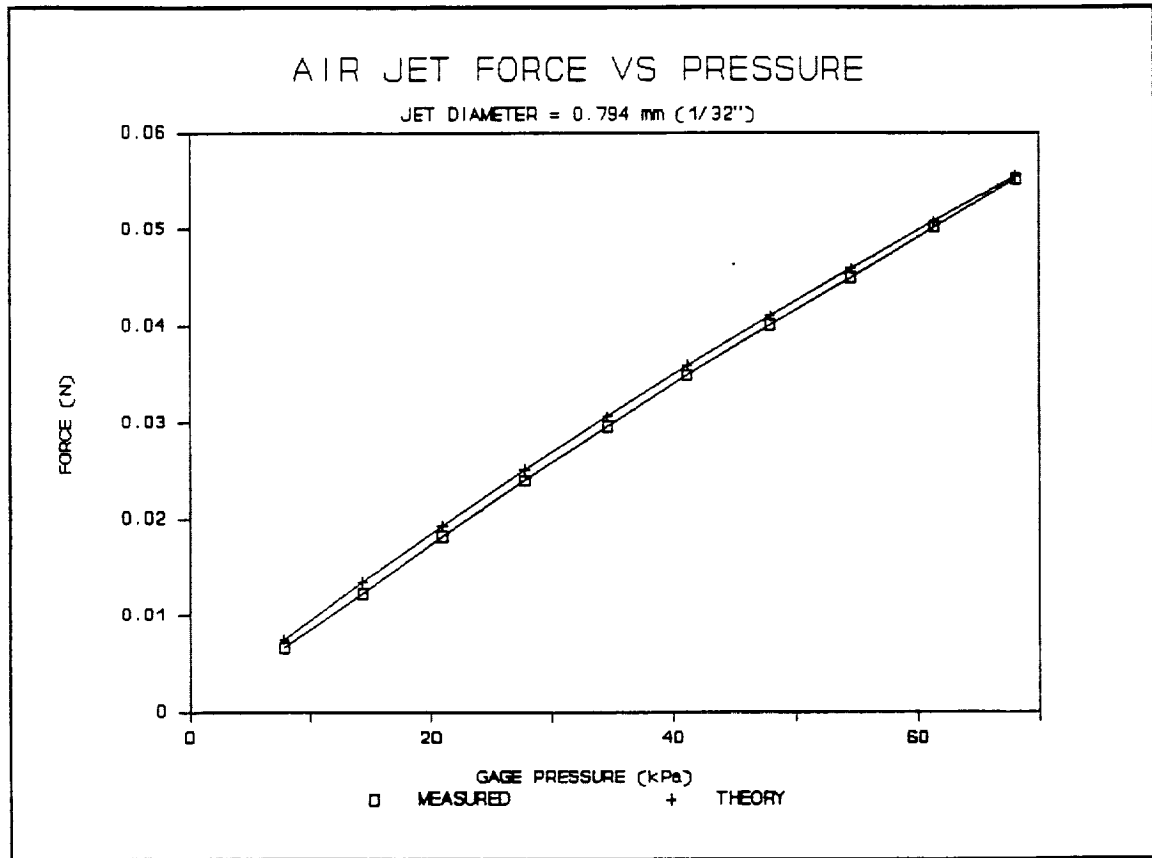
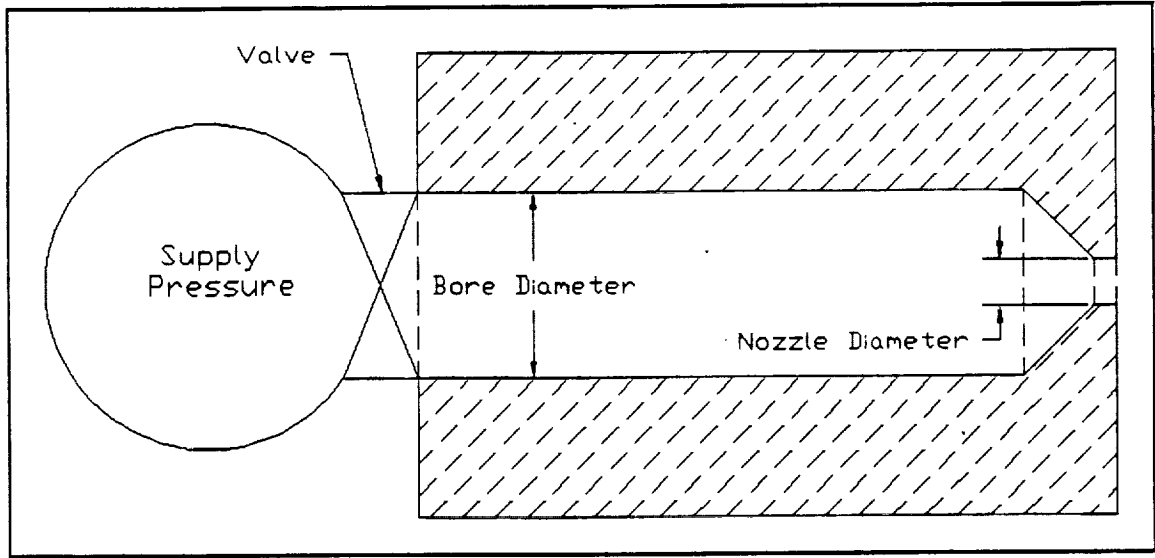
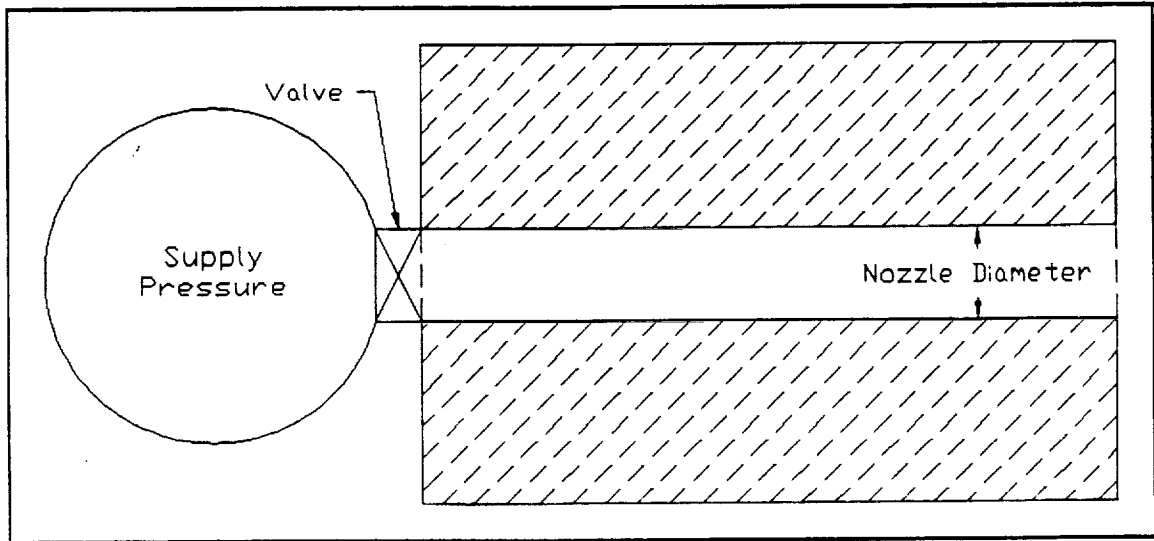


Figure 12 Comparison of Predicted and Measured Forces with Nozzle Diameter of 0.794 mm (1/32")



**Figure 13 Section View of Small Nozzles**



**Figure 14 Section View of Large Nozzles**

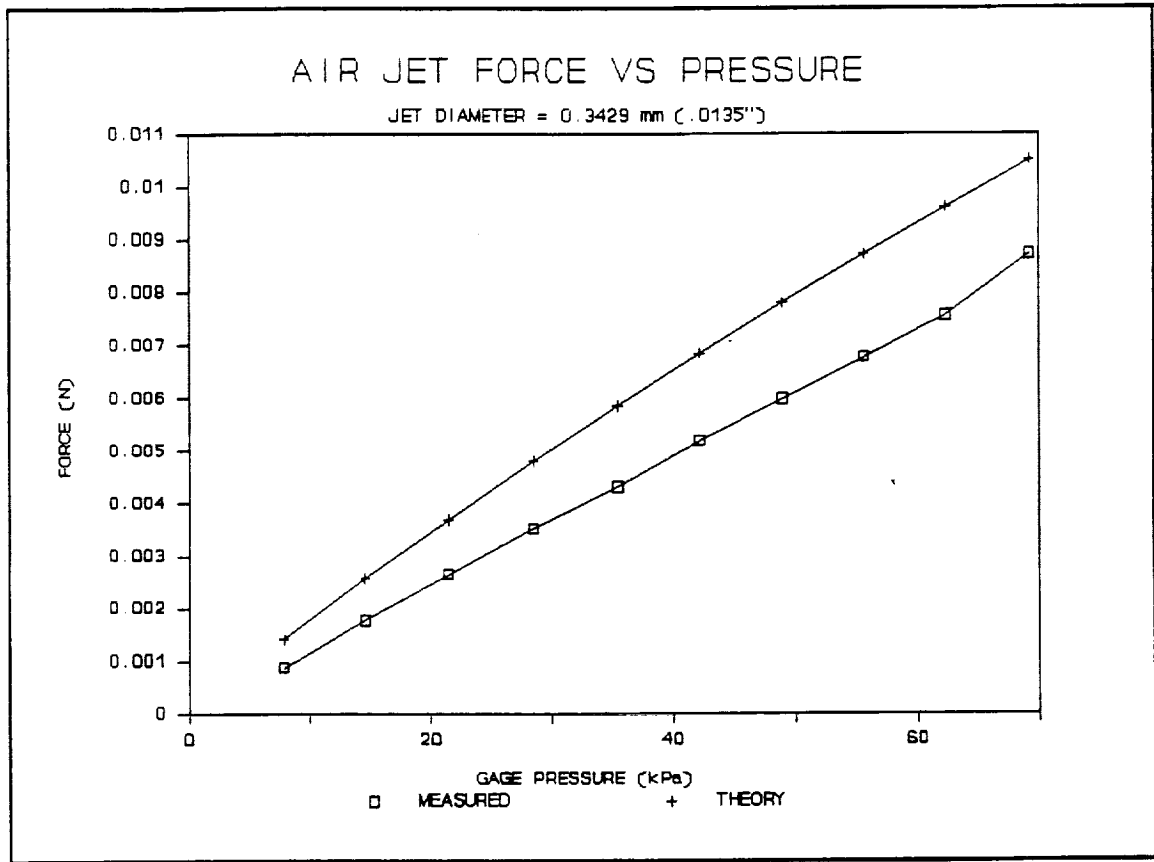
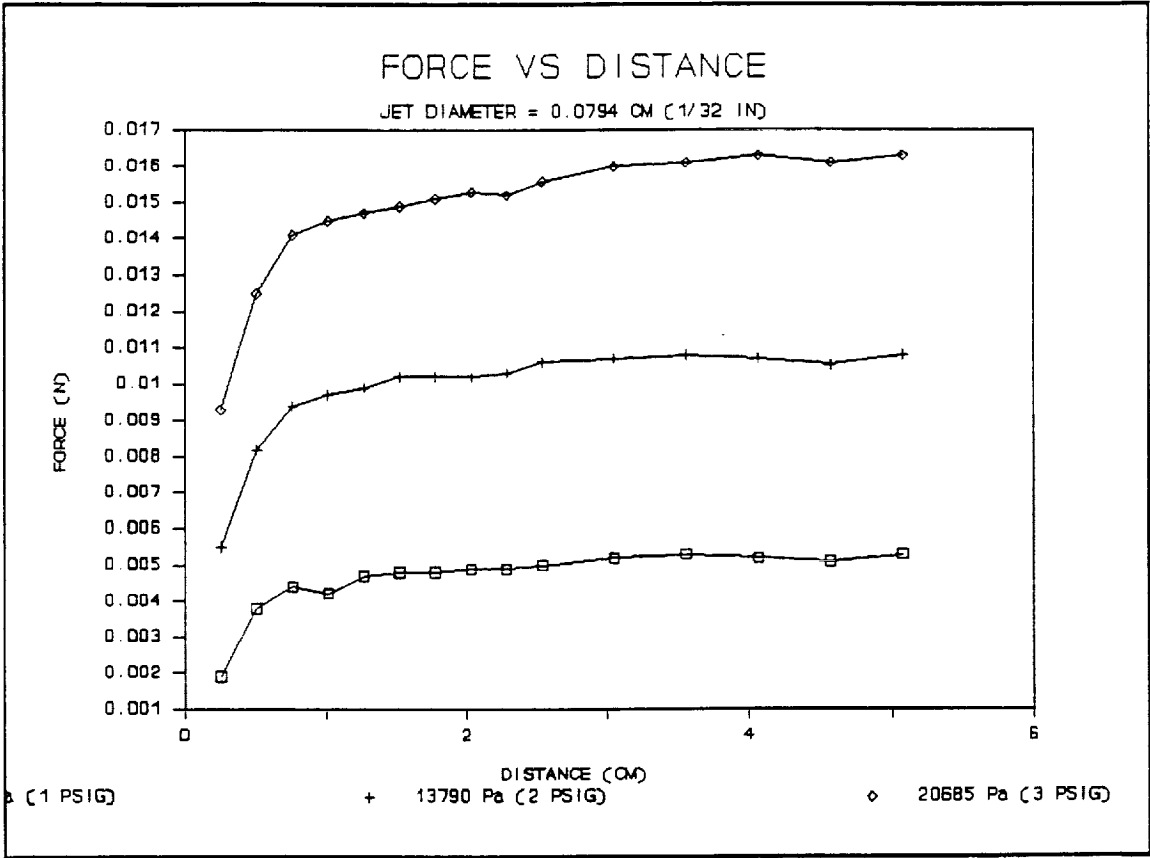
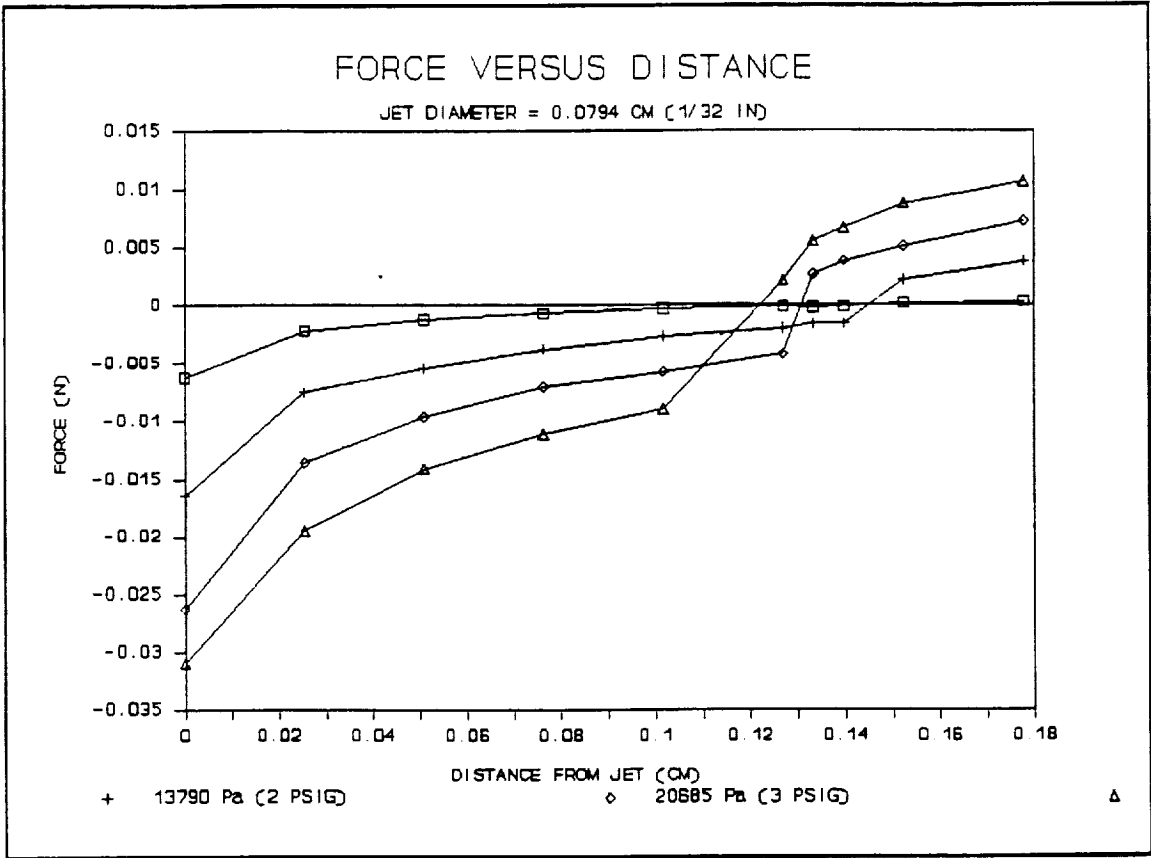


Figure 15 Comparison of Predicted and Measured Forces with Nozzle Diameter of 0.343 mm (0.0135")



**Figure 16 Relationship of Air Jet Forces with Distance from the Jet**



**Figure 17** Illustration of Bernoulli Effects on Air Jet Forces

#### D. Analytical Model

A mathematical model was developed to predict dynamic response of the payload in both one-dimensional and planar motion. Analytical and experimental results were compared to establish system parameters and validate the model. The analytical model was then used to predict payload acceleration levels resulting from typical Space Station disturbances.

##### One-dimensional motion

The mathematical model for one-dimensional motion was developed using the single degree-of-freedom spring-mass-damper system shown in figure 18 to represent the experimental setup depicted in figure 19. The four springs shown in figure 19 were incorporated into one equivalent spring, and the damper includes viscous friction of the air bearings and internal damping of the springs. The equation of motion for the model in figure 18 is

$$M\ddot{X}_2 = -K(X_2 - X_1) - C(\dot{X}_2 - \dot{X}_1) - F(t)$$

where  $M$  = payload mass,  $K$  = spring rate of the helical springs, and  $C$  = damping coefficient. To validate the mathematical model with experimental results, the base motion,  $X_1$ , which represents the motion of the frame in the experimental setup, is set to zero, reducing the equation to

$$\ddot{X} + 2\zeta\omega_n\dot{X} + \omega_n^2X = F(t)$$

where  $X = X_2$ . The damping ratio,  $\zeta$ , was obtained from the logarithmic decrement

$$\ln(A_1/A_2) = (2\pi\zeta) / \sqrt{1 - \zeta^2}$$

where  $A_1$  and  $A_2$  are the amplitudes of two consecutive cycles. Assuming that  $\zeta^2$  is small compared to one, the equation can be rewritten as,

$$\zeta = \ln(A_1/A_2) / 2\pi$$

The damped natural frequency,  $\omega_d$ , was found from

$$\omega_d = 2\pi (\text{number of cycles/total time})$$

The undamped natural frequency is related to the damped natural frequency by

$$\omega_n = \omega_d / \sqrt{1 - \zeta^2}$$

Since  $\zeta^2$  is small it is apparent that the damped and undamped natural frequencies are virtually identical.

## Planar motion

The experimental setup was modified to allow planar motion. In order for the effect of the air jet forces on the payload response to be made more dominant, the spring rates were reduced. The four springs were replaced by one spring on each side of the payload, reducing the total spring rate of the system. The individual spring rates were also decreased by adding more active coils. The number of active coils was changed from 8 to 16, which halved the spring rate.

In planar motion there are three degrees-of-freedom. The coordinates chosen to represent the system and a schematic of the planar model are shown in figure 20. The system was modeled with one spring on each side of the payload acting along the vectors  $R_1$  and  $R_2$ . The hose which supplied air to the air-bearing cart was assumed to have a negligible spring rate in all directions. It is important to note that the origin of the coordinate system lies at the equilibrium point of the center of mass of the payload. With these assumptions, the equations of motion are

$$\begin{aligned}
 M\ddot{X} &= -K(|R_1|^{-1}l_u)\cos\phi_1 - K(|R_2|^{-1}l_u)\cos\phi_2 - C\dot{R}_{1x} - C\dot{R}_{2x} + F_1 \\
 M\ddot{Y} &= -K(|R_1|^{-1}l_u)\sin\phi_1 - K(|R_2|^{-1}l_u)\sin\phi_2 - C\dot{R}_{1y} - C\dot{R}_{2y} + F_2 + F_3 \\
 I\ddot{\theta} &= Kr_x(|R_1|^{-1}l_u)(-\sin\theta\sin\phi_1 - \cos\theta\cos\phi_1) \\
 &\quad + Kr_x(|R_2|^{-1}l_u)(\sin\theta\sin\phi_2 + \cos\theta\cos\phi_2) \\
 &\quad - Cr_x(\dot{R}_{1x}\cos\theta + \dot{R}_{1y}\sin\theta) + Cr_x(\dot{R}_{2x}\cos\theta + \dot{R}_{2y}\sin\theta) \\
 &\quad + F_1Y - F_2(\Delta+X) + F_3(\Delta-X)
 \end{aligned}$$

where,

$$\phi_1 = -\tan^{-1}(R_{1x}/R_{1y}) + \pi/2$$

$$\phi_2 = -\tan^{-1}(R_{2x}/R_{2y}) - \pi/2$$

$$R_1 = (X+r_y\sin\theta-x)i + (D+Y-r_y\cos\theta-x)j$$

$$R_2 = (X-r_y\sin\theta-x)i + (-D+Y+r_y\cos\theta+x)j$$

$$\dot{R}_1 = (\dot{X}+r_y\dot{\theta}\cos\theta-\dot{x})i + (\dot{Y}+r_y\dot{\theta}\sin\theta-\dot{x})j$$

$$\dot{R}_2 = (\dot{X}-r_y\dot{\theta}\cos\theta-\dot{x})i + (\dot{Y}-r_y\dot{\theta}\sin\theta+\dot{x})j$$

$\Delta$  = distance of sensor to origin of coordinate system

$x$  = external disturbance of the frame

$l_u$  = unstretched length of spring

$r_x$  = distance from center of mass to side of payload in the X direction

$r_y$  = distance from center of mass to side of payload in the Y direction

D = distance from frame to side of payload in the Y direction

$F_i$  = ith jet force

These equations were developed for a symmetric system with no elastic or dynamic coupling. To account for coupling that was observed in the experimental system coupling terms were added to the equations of motion as follows:

$$\begin{aligned} M\ddot{X} &= -K(|R_1|-l_u) - K(|R_2|-l_u)\cos\phi_2 - C\dot{R}_{1x} \\ &\quad - C\dot{R}_{2x} + F_1 + \epsilon Y + \beta\theta \\ M\ddot{Y} &= -K(|R_1|-l_u)\sin\phi_1 - K(|R_2|-l_u)\sin\phi_2 - C\dot{R}_{1y} \\ &\quad - C\dot{R}_{2y} + F_2 + F_3 + \epsilon X + \alpha\theta \\ I\ddot{\theta} &= Kr_x(|R_1|-l_u)(\sin\theta\sin\phi_1 - \cos\theta\cos\phi_1) + \\ &\quad Kr_x(|R_2|-l_u)(\sin\theta\sin\phi_2 + \cos\theta\cos\phi_2) - \\ &\quad Cr_x(\dot{R}_{1x}\cos\theta + \dot{R}_{1y}\sin\theta) + Cr_x(\dot{R}_{2x}\cos\theta + \dot{R}_{2y}\sin\theta) + \\ &\quad F_1 Y - F_2(\Delta+X) + F_3(\Delta-X) + \beta X + \alpha Y \end{aligned}$$

where,

$\alpha$  = coupling coefficient between Y and  $\theta$

$\beta$  = coupling coefficient between X and  $\theta$

$\epsilon$  = coupling coefficient between X and Y

Since the coupling was assumed to be due only to the elastic restoring forces, Maxwell's law of reciprocity applies and each coupling term was placed in the respective equations, i.e. the  $\alpha$  term in the Y and  $\theta$  equations, the  $\beta$  term in the X and  $\theta$  equations and the  $\epsilon$  term in the X and Y equations. The coupling observed in the experiment could be caused by several peculiarities in the experimental setup. The springs may not act directly through the center of mass of the payload, which could cause coupling in X and

$\theta$  or  $Y$  and  $\theta$ . If the spring forces do not act through the center of mass, coupling in the  $X$  and  $Y$  directions will occur. The weight of the springs themselves act as "gravity springs" causing small perturbations in all three directions. The spring rate of the springs on the experimental system was extremely low compared to their weight, causing them to sag. When a string was connected from the frame to the center of the length of the spring to support it, the coupling terms were reduced but not eliminated completely. It was assumed that the springs behaved linearly, or at least operated in a linear region. Any one, or more likely a combination of these factors, could affect the coupling of the system. However, the coupling effects are small, and the values of the coupling coefficients,  $\alpha$ ,  $\beta$ ,  $\epsilon$  used in the analytical model are a small percentage of the spring rates.

The jet forces have been discussed in the Pneumatic System Modeling section on p. 19. Since there are three degrees-of-freedom, there must be three forces to control the motion of the payload. Figure 20 shows the positioning of the control forces. The air jets impinge on the sides of the payload causing the control forces to keep it centered. If the air does not strike normal to the payload a tangential force component exists. It is assumed that the tangential components are negligible since the angular motion is small.

Because the sensors do not detect motion of the center of mass of the payload, variables  $X$ ,  $Y$ , and  $\theta$  must be calculated from the sensor readings. Figure 21 presents a schematic from which the following trigonometric relations between the sensor readings and the variables were developed :

$$\delta_1 = X + r_x((1/\cos\theta)-\cos\theta) + Y\tan\theta$$

$$\delta_2 = r_y(1-\cos\theta) - r_x\tan\theta - r_y(1/\cos\theta-\cos\theta)+Y$$

$$\delta_3 = r_y(1-\cos\theta) + r_x\tan\theta - r_y(1/\cos\theta-\cos\theta)+Y$$

### Experimental setup natural frequencies and damping

Natural frequencies and damping ratios for the three degree-of-freedom system were found experimentally; the values were used to establish parameters for the analytical model. The damping ratio could not be determined from the logarithmic decrement as in the one-dimensional case due to coupling between  $X$ ,  $Y$ , and  $\theta$ . The decay of the total energy of the system was used to find the damping ratio (Cordera, 1989). The damping ratio,  $\zeta$ , and the natural frequency were determined to be 0.017 and 0.2398 rad/s (0.0382 Hz) respectively. These values were virtually the same in the  $X$  and  $Y$  directions. The rotational natural frequency was 0.393 rad/s (0.0625 Hz) and the damping ratio was close to the 0.017 value determined for translational motion. The damping coefficient

and the spring rate were then calculated to be 0.13 N-s/m and 0.92 N/m respectively for each spring. The payload mass was 32 kg, and the mass moment of inertia, determined by suspending the payload as a quadrafilar pendulum, was measured to be 1.15 kg-m<sup>2</sup>.

### System simulation

The analytical models of payload dynamics, control logic and air jet forces were combined into a system simulation. A software package known as Advanced Continuous Simulation Language, ASCL, was used to aid in the simulation of the system. The computer program for the analytical model was carefully designed to match the information flow process and logic established for the experimental setup. For example, sensor signals were calculated, sent through a low pass filter, then numerically differentiated to obtain velocity. A decision was made on which control forces should be applied, then the acceleration of the three state variables (X, Y and  $\theta$ ) was determined. These accelerations were integrated numerically twice to obtain displacements. The maximum acceleration of the payload was calculated assuming that it would occur at one of the four corners of the payload.

ORIGINAL PAGE IS  
OF POOR QUALITY

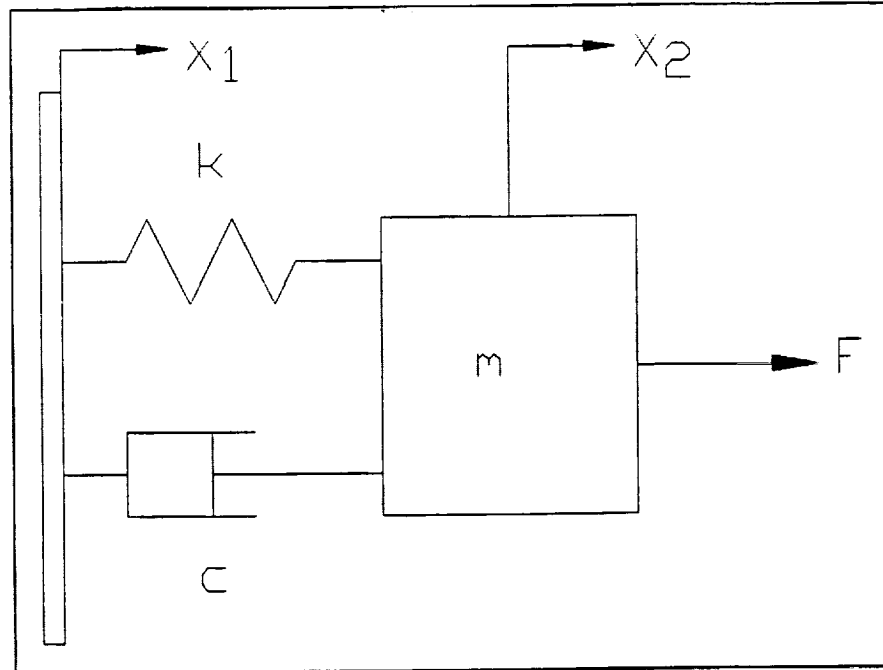


Figure 18 Single Degree-of-Freedom Model

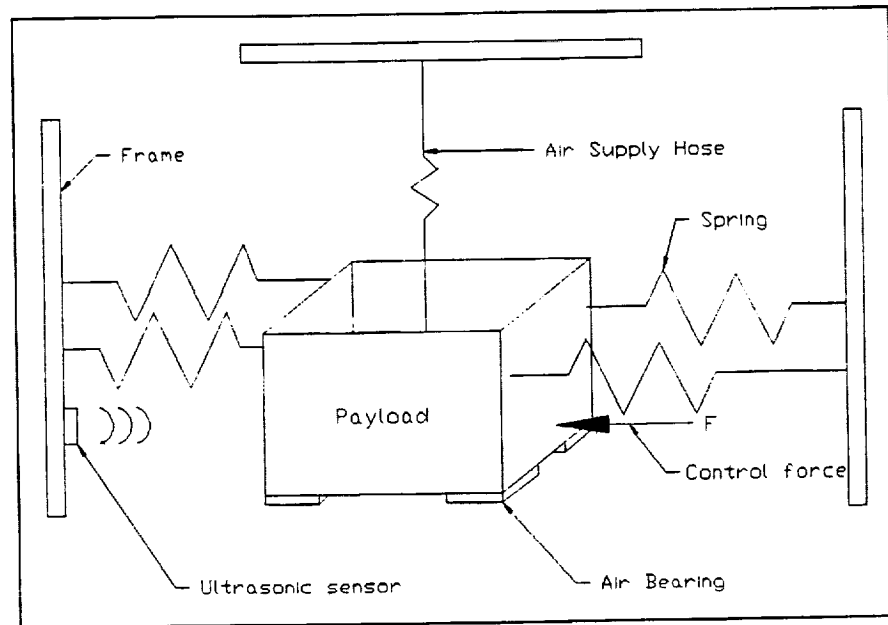


Figure 19 Schematic of Test Setup for One-dimensional Motion

ORIGINAL PAGE IS  
OF POOR QUALITY

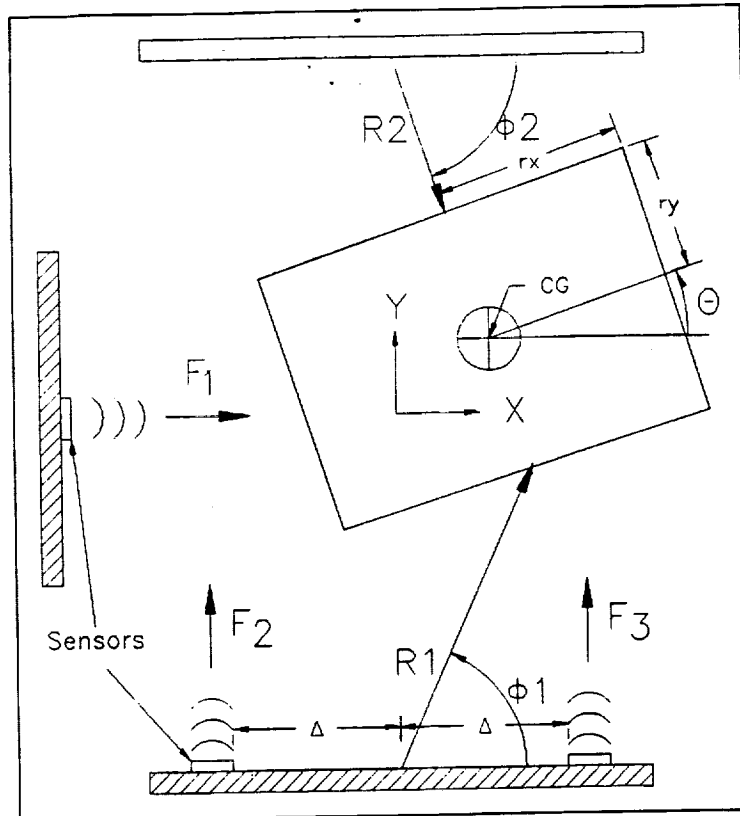


Figure 20 Top View of Experiment and Coordinates Chosen

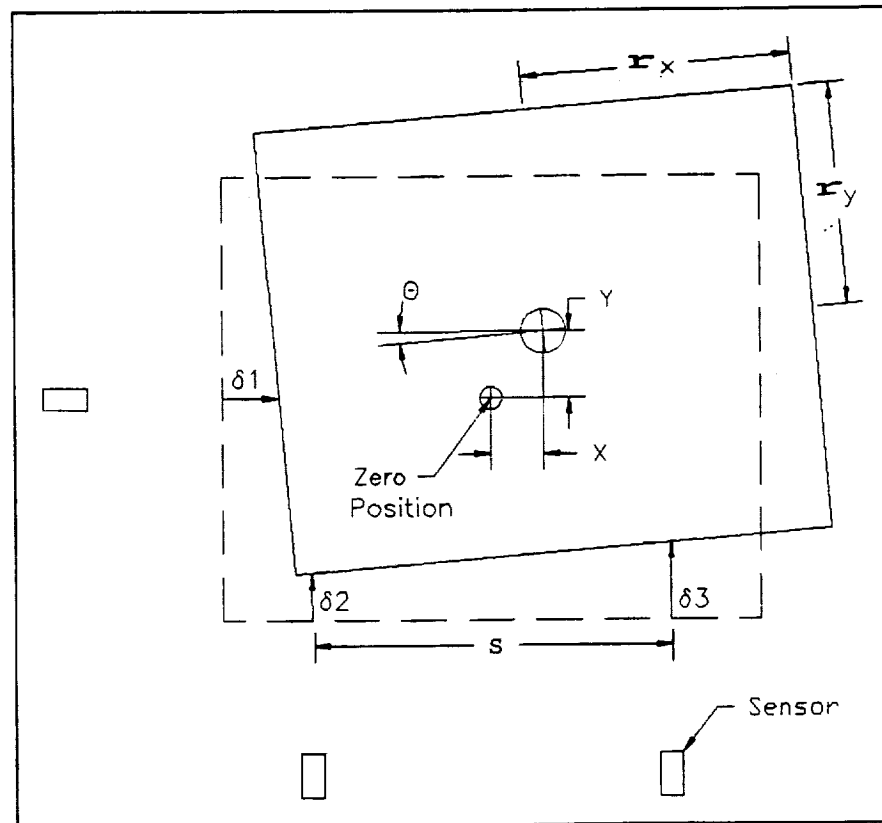


Figure 21 Relationship of Control Variables to Sensors

## V. BASIC DATA GENERATED and SIGNIFICANT RESULTS

To verify the two - dimensional analytical model experimental and predicted payload response were compared. Experimental tests included:

- i) Predominant one-dimensional payload motion in the X, Y, and  $\theta$  directions;
- ii) General plane motion.

Experimental tests and theoretical simulations were conducted using the 0.343 mm (0.0135") jet diameter and an upstream pressure of 34.5 kPa (5 psi) gauge. Once the analytical model was verified it was used to simulate payload response to harmonic and impulse loading. Response to these types of loads could not be verified experimentally due the lack of necessary instrumentation to measure in the micro-g range.

### Free vibration

Before the controllers were implemented, characteristics of the uncontrolled system were determined from free vibration tests. These tests served two purposes. First, to establish analytical model parameters, and secondly, to guide the development of the coupling terms in the equations of motion and other details of the analytical model.

Figures 22 and 23 show results of a free vibration in the Y direction with an initial displacement in the Y direction. The analytical model produces an accurate prediction of the experimental response except for slight differences in the coupling between the X and Y motion, as shown in figures 24 and 25. Notice that initially X is not excited but becomes excited as the test progresses. This was found to be a typical result between X and Y motion. Reasons for the coupling are discussed in the Analytical Model section on p. 29. Coupling is not a major concern since it is a characteristic of this particular experimental setup. The role and nature of coupling that may exist is system dependent. Figures 26 and 27 provide a comparison of the rotational motion for free vibration. Negligible coupling was found between X and  $\theta$  and Y and  $\theta$ .

### Displacement control

Displacement control was initially chosen for its ability to completely damp the system motion to within a given dead band to meet acceleration requirements. Figures 28 and 29 give results from an experimental and theoretical test in the X direction. These figures show the system motion to be completely damped, as expected, to within the 0.5 mm dead band used. A comparison of these results to those of free vibration, Figures 30 and 31, demonstrates the effectiveness of this controller. These results are exhibited by both the analytical model and the experiment. One of the original concerns with the two-dimensional system was how well the rotational motion could be controlled. Figures 32 and 33

show that rotation can be controlled effectively. The time needed to reduce the oscillation to the required level was found to be greater than the time to reduce the translational motion. This was attributed to the large mass moment of inertia as compared to the small control moments.

Adequate performance of the displacement controller for single degree-of-freedom motion has been demonstrated. While these one-dimensional tests provide a useful comparison of control effectiveness between the different controllers, the primary objective here is to demonstrate control for two-dimensional motion. Several tests were conducted in which the payload was given an arbitrary initial displacement that would excite all three modes of vibration. Response is similar to the single degree-of-freedom response except coupling between X and Y is present. The displacement controller proved to be as effective in controlling planar motion as it was in controlling one-dimensional motion.

### Velocity control

The velocity control scheme was expected to damp the payload more quickly than with the displacement controller since for simple harmonic payload motion the controller is activated a greater percentage of each cycle, thus removing energy more rapidly. Figures 34 and 35 show this behavior for a test in the X direction. Only a few cycles occur before the payload is held within the velocity dead band (1 mm/s). The problem with this controller was that the large velocity dead band needed to avoid the effects (solenoid chatter) of noise resulted in the system not being damped to an acceptable amplitude. Also, during the progress of the same test Y becomes excited, much as during free vibration. Figures 36 and 37 show results for a test with only rotational motion. Again, extensive two-dimensional testing demonstrated that the velocity controller performed as expected for general plane motion.

### Combinational control

The combinational control scheme was designed to take advantage of the high damping rate of the velocity controller and the ability to completely damp the payload as achieved by the displacement controller. Tests and analytical results demonstrated both these characteristics. Figures 38 and 39 provide an example of the combinational controller for a single degree-of-freedom test in the X direction. Notice the system response is much quicker than with displacement control alone while the motion is damped to the desired amplitude. Figures 40 and 41 demonstrate the combinational control for rotational motion. The rotational motion, as with the other controllers, requires more time to damp completely. Comparisons of the experimental and analytical results for two-dimensional motion again displayed a favorable comparison between theory and experiment.

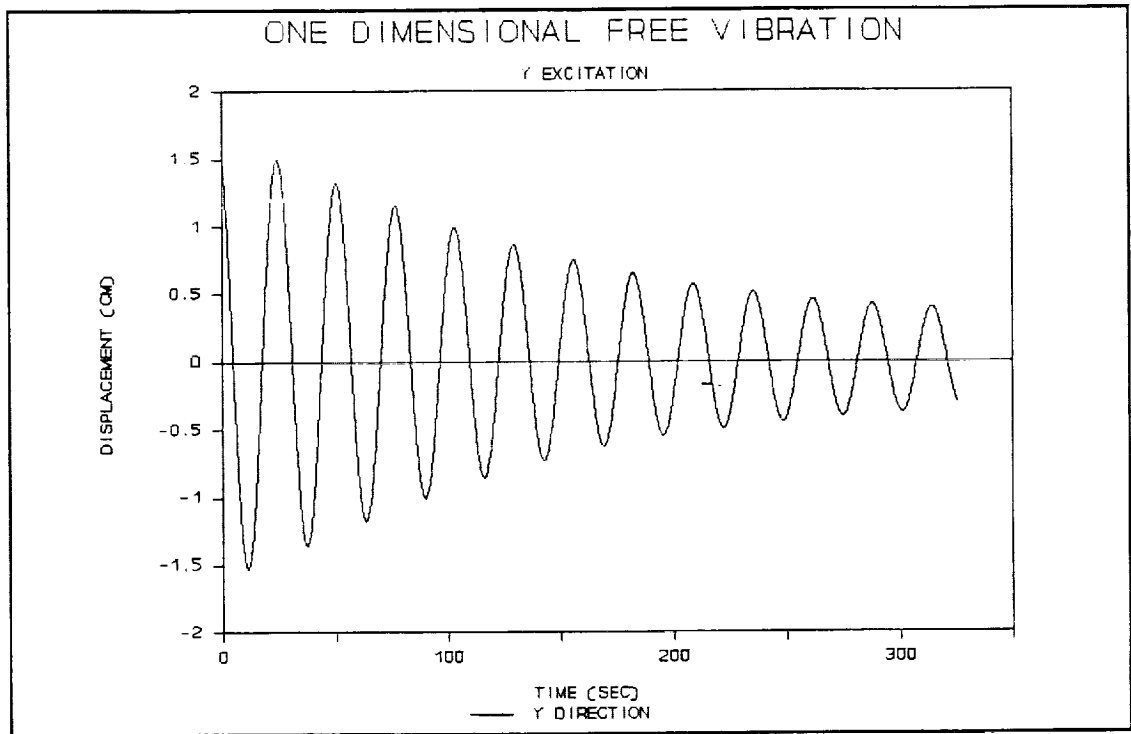


Figure 22 Experiment: Free Vibration, Y IC, Y Dir

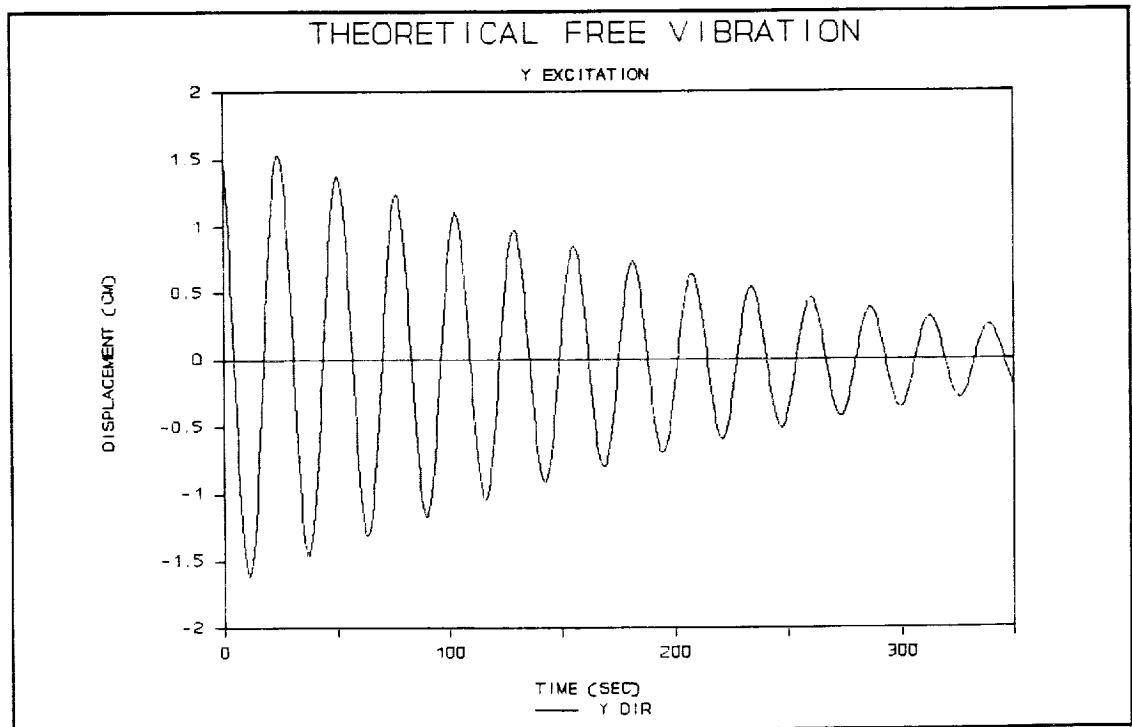


Figure 23 Theory: Free Vibration, Y IC, Y Dir

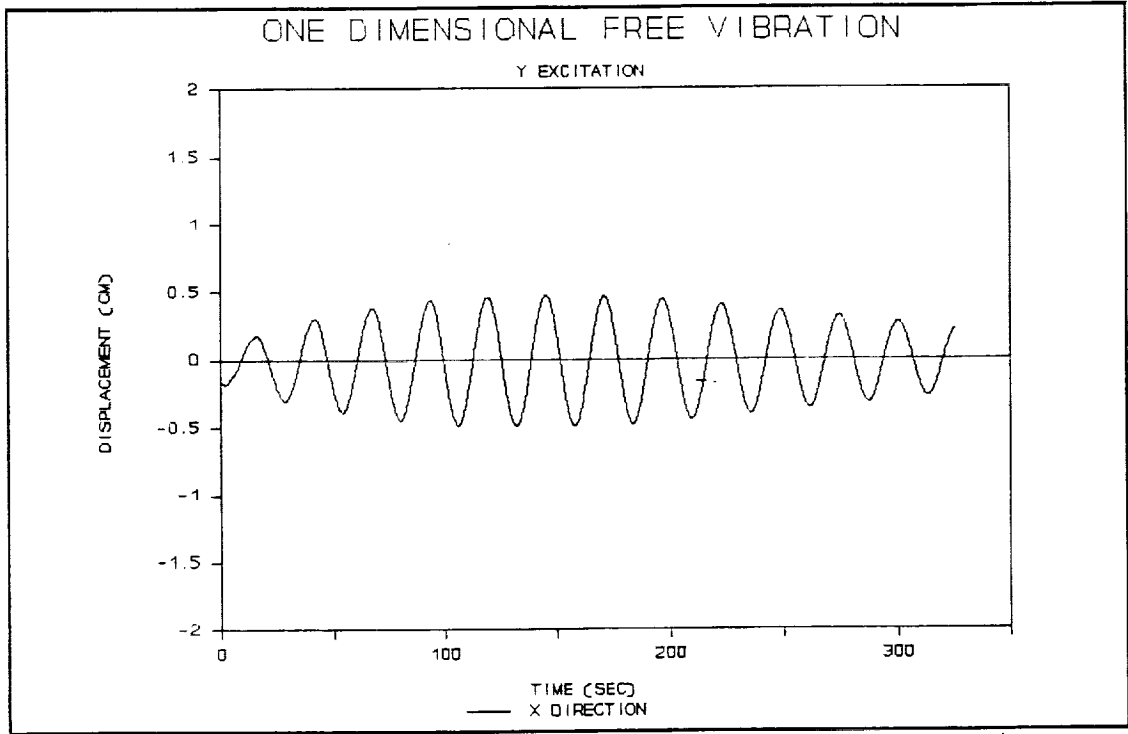


Figure 24 Experiment: Free Vibration, Y IC, X Dir

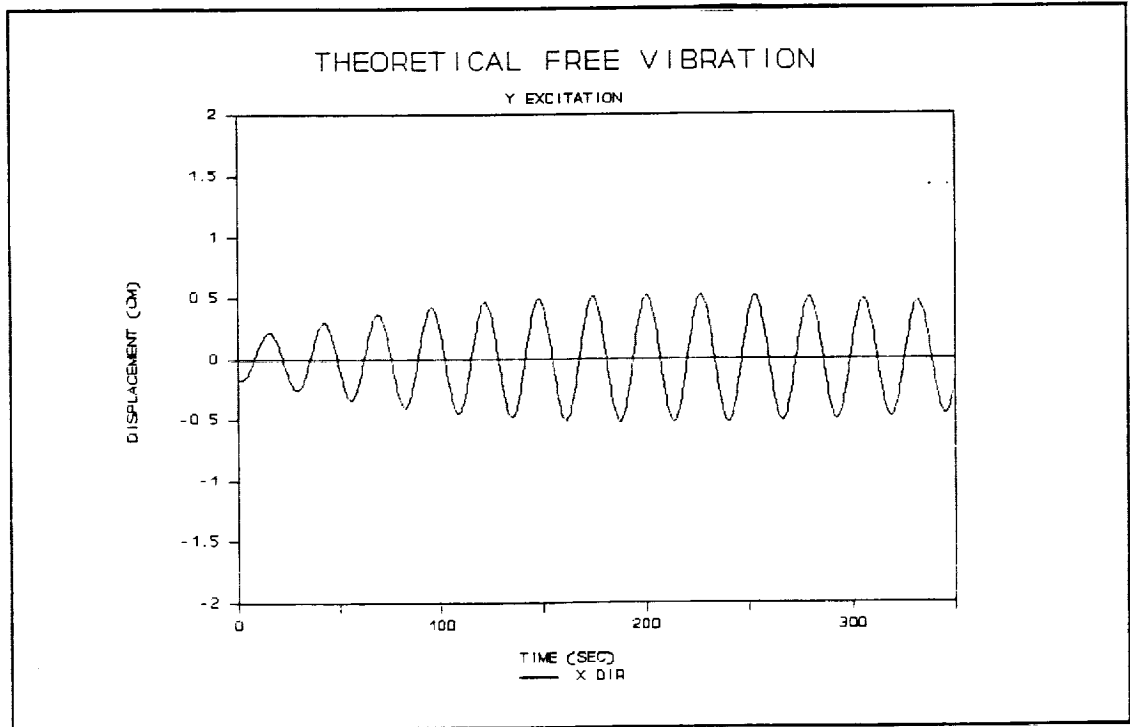


Figure 25 Theory: Free Vibration, Y IC, X Dir

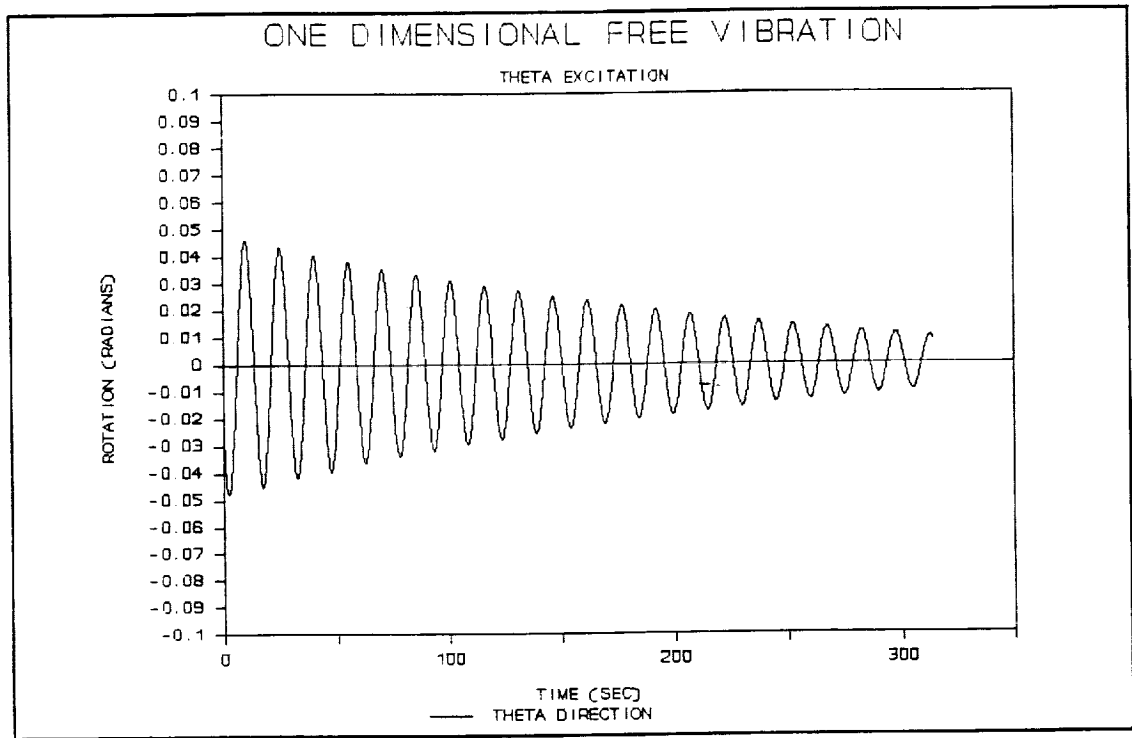


Figure 26 Experiment: Free Vibration,  $\theta$  IC,  $\theta$  Dir

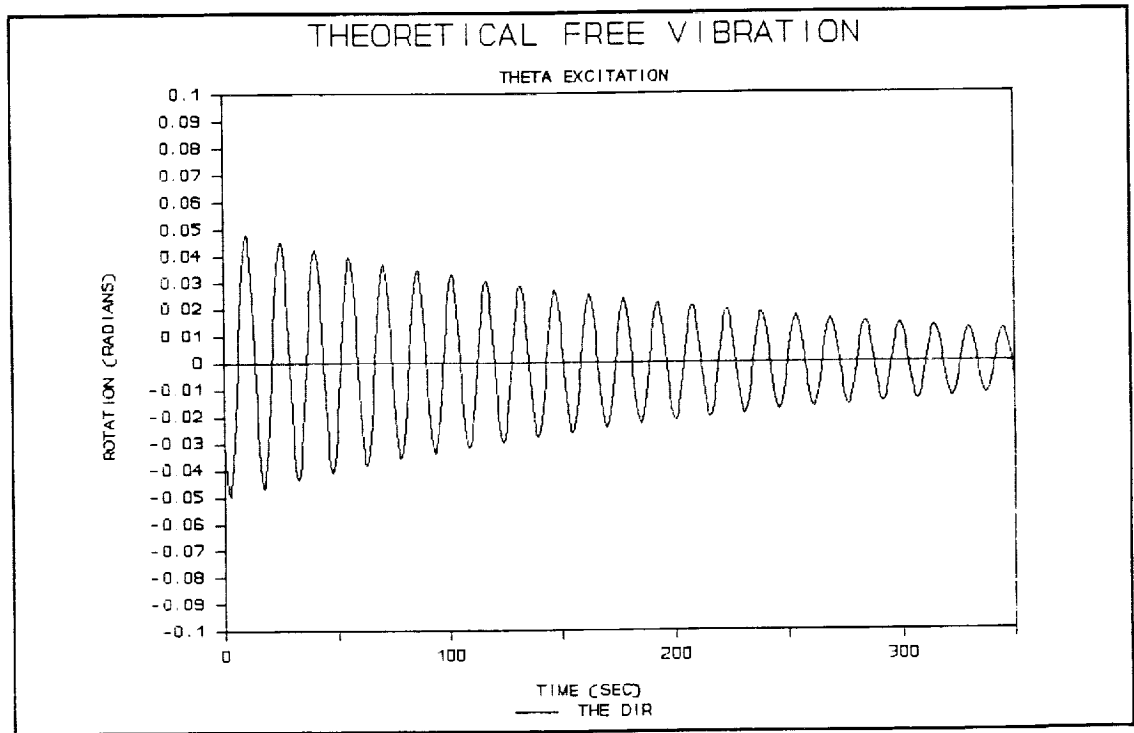


Figure 27 Theory: Free Vibration,  $\theta$  IC,  $\theta$  Dir

ORIGINAL PAGE IS  
OF POOR QUALITY

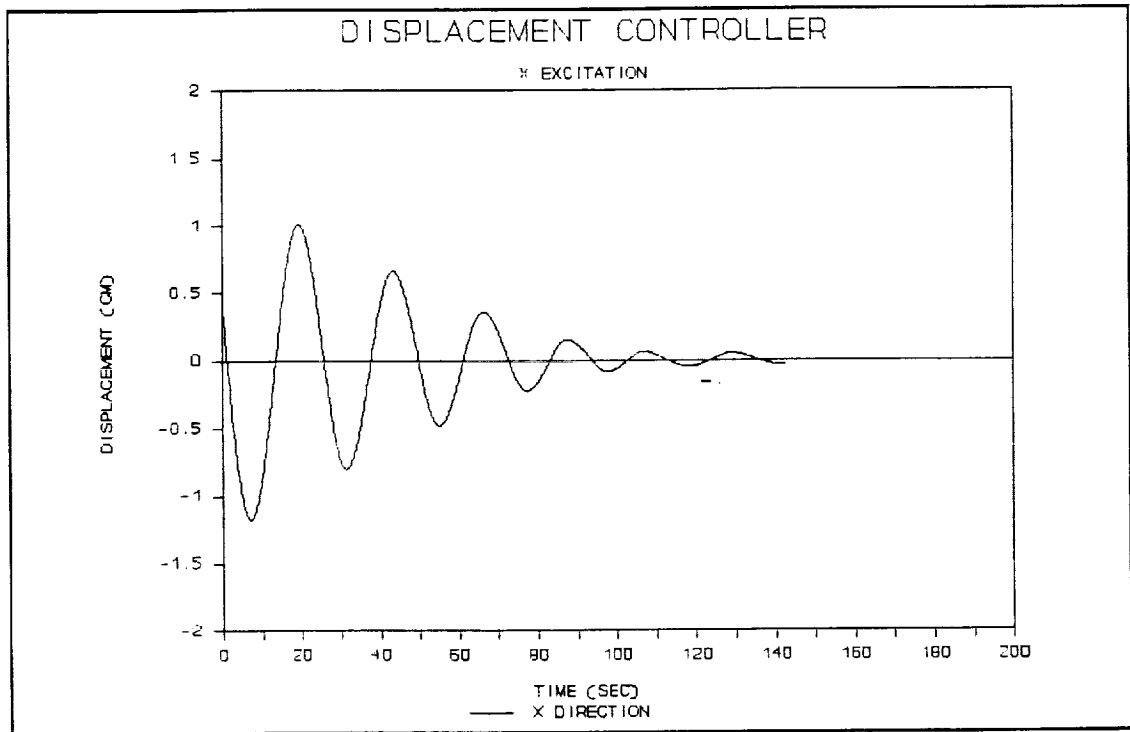


Figure 28 Experiment: Displacement Control, X IC, X Dir

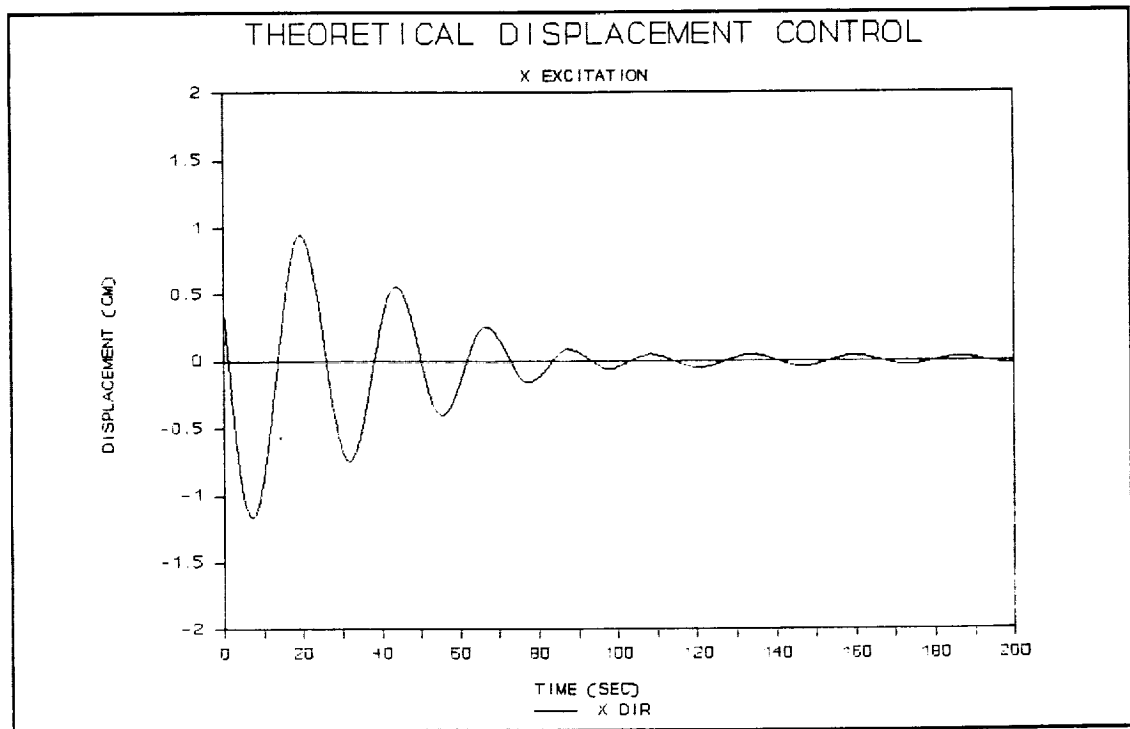


Figure 29 Theory: Displacement Control, X IC, X Dir

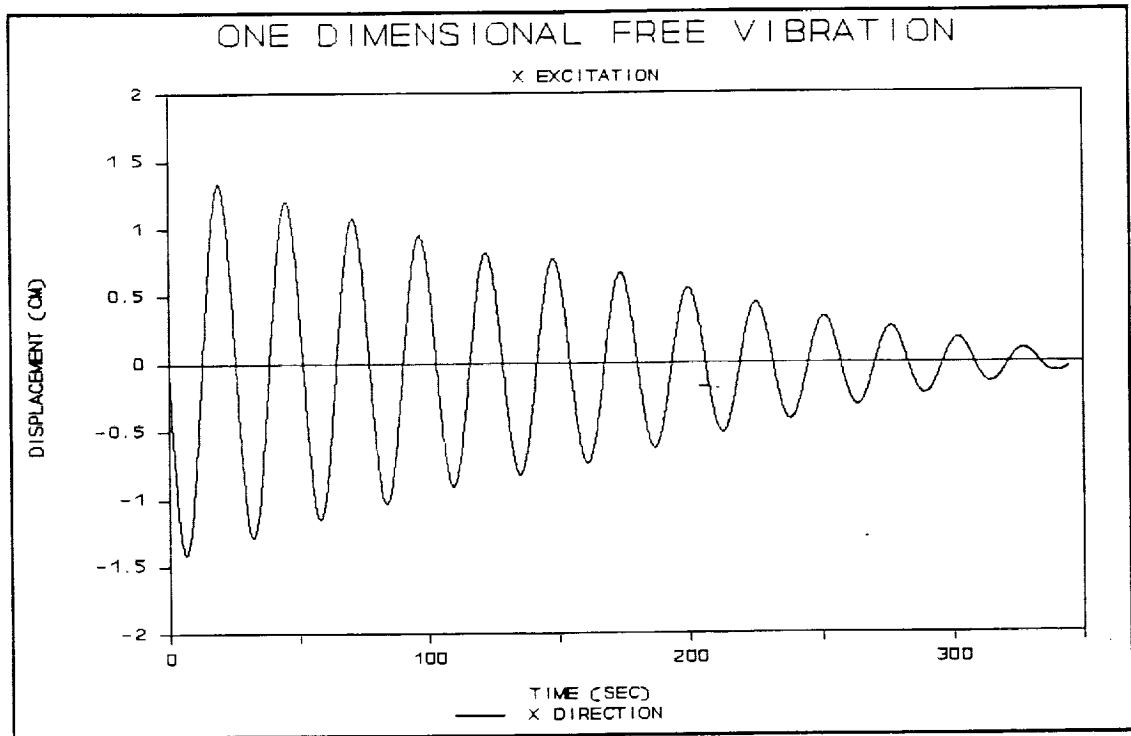


Figure 30 Experiment: Free Vibration, X IC, X Dir

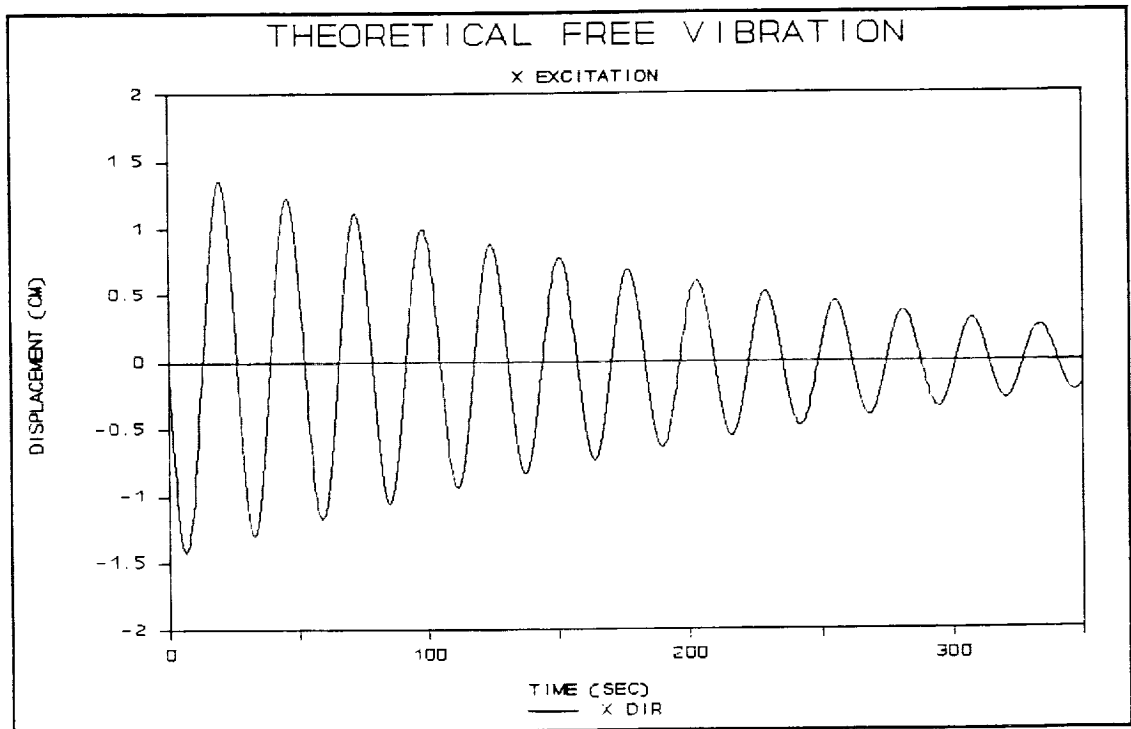


Figure 31 Theory: Free Vibration, X IC, X Dir.

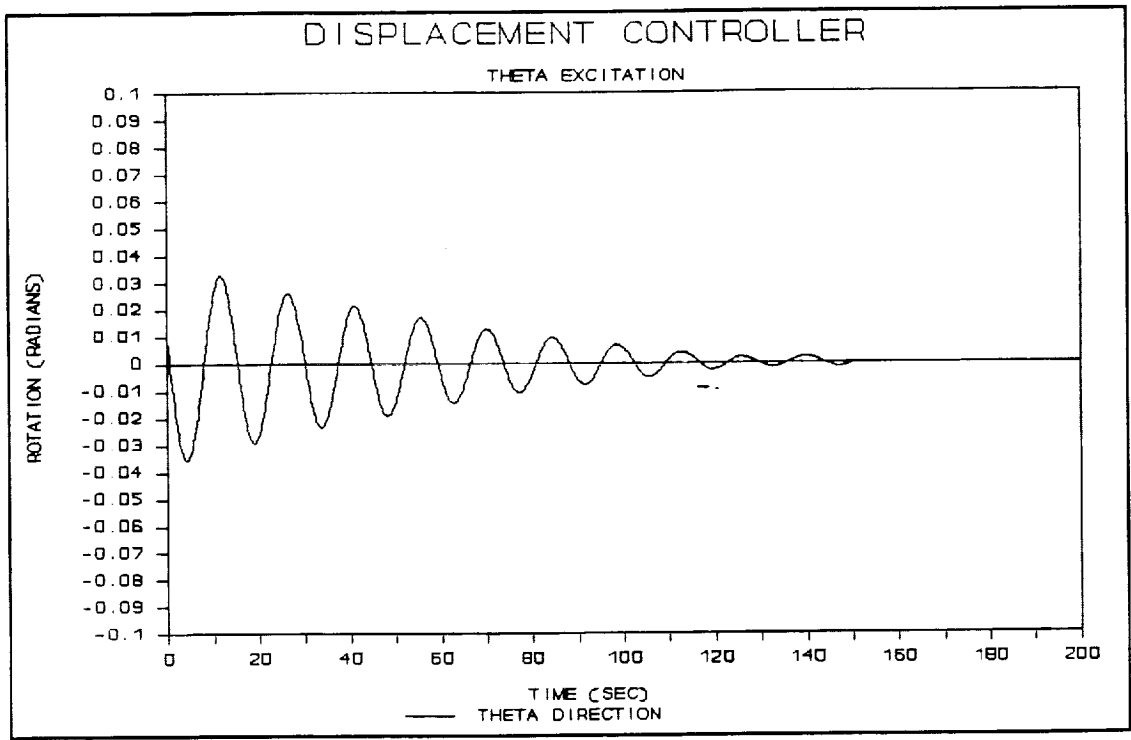


Figure 32 Experiment: Displacement Control,  $\theta$  IC,  $\theta$  Dir

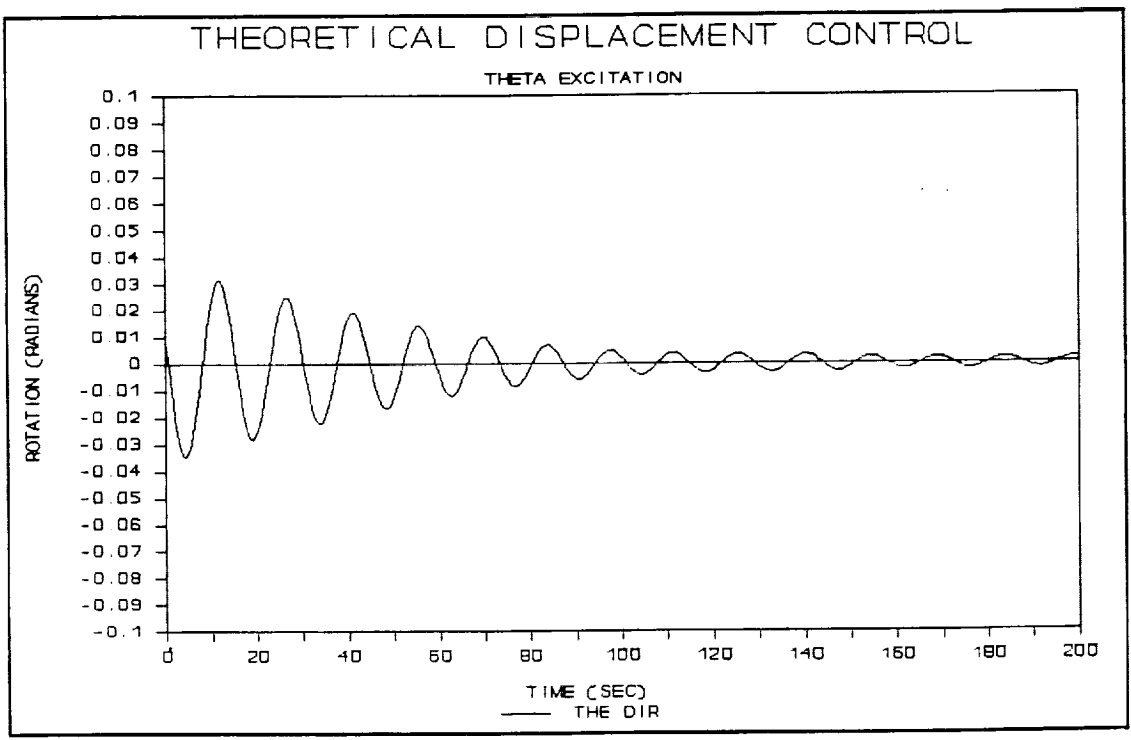


Figure 33 Theory: Displacement Control,  $\theta$  IC,  $\theta$  Dir

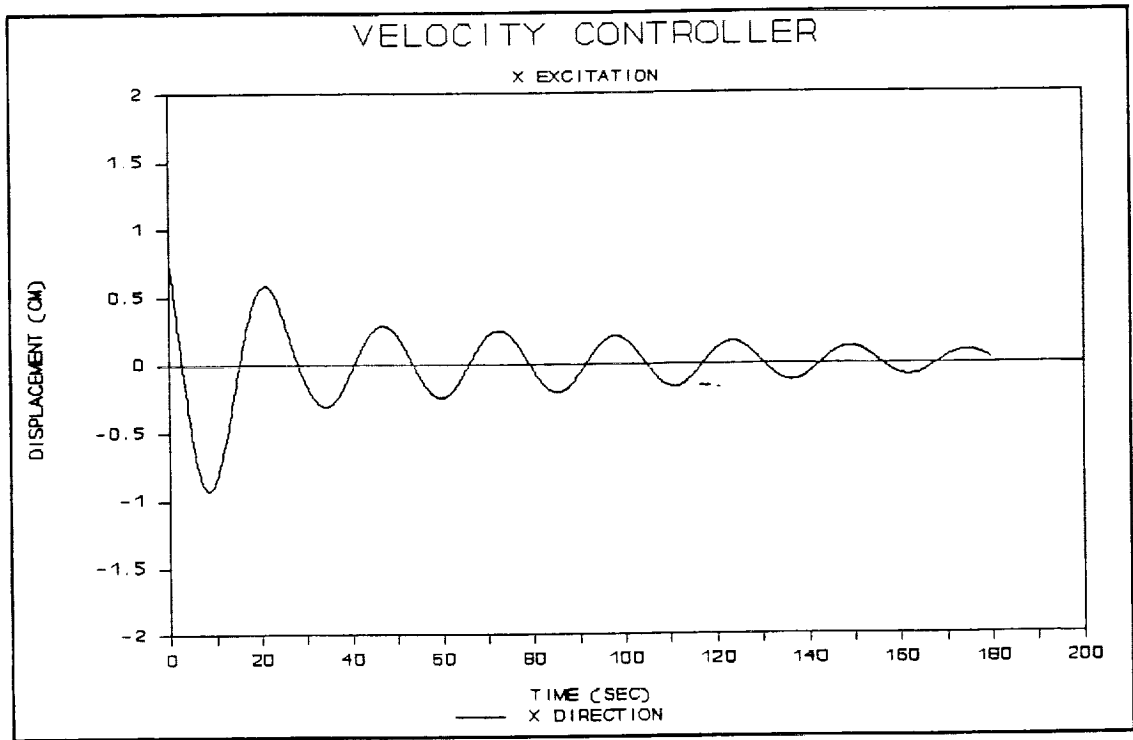


Figure 34 Experiment: Velocity Control, X IC, X Dir

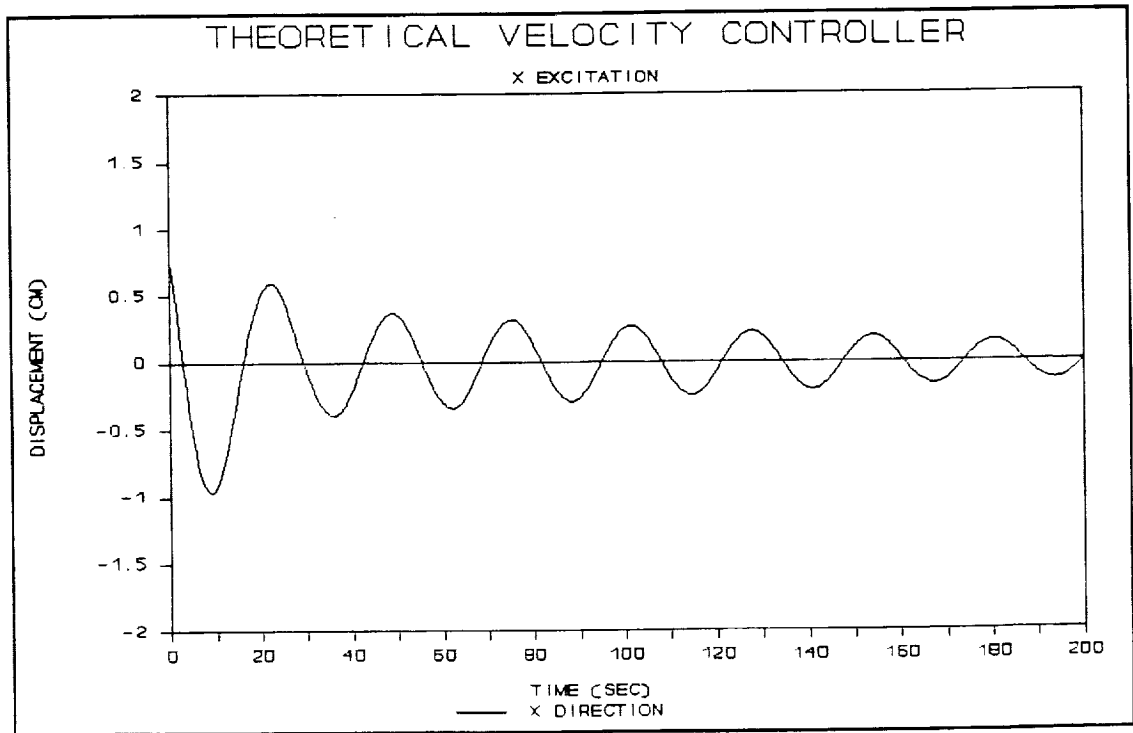


Figure 35 Theory: Velocity Control, X IC, X Dir

ORIGINAL PAGE IS  
OF POOR QUALITY

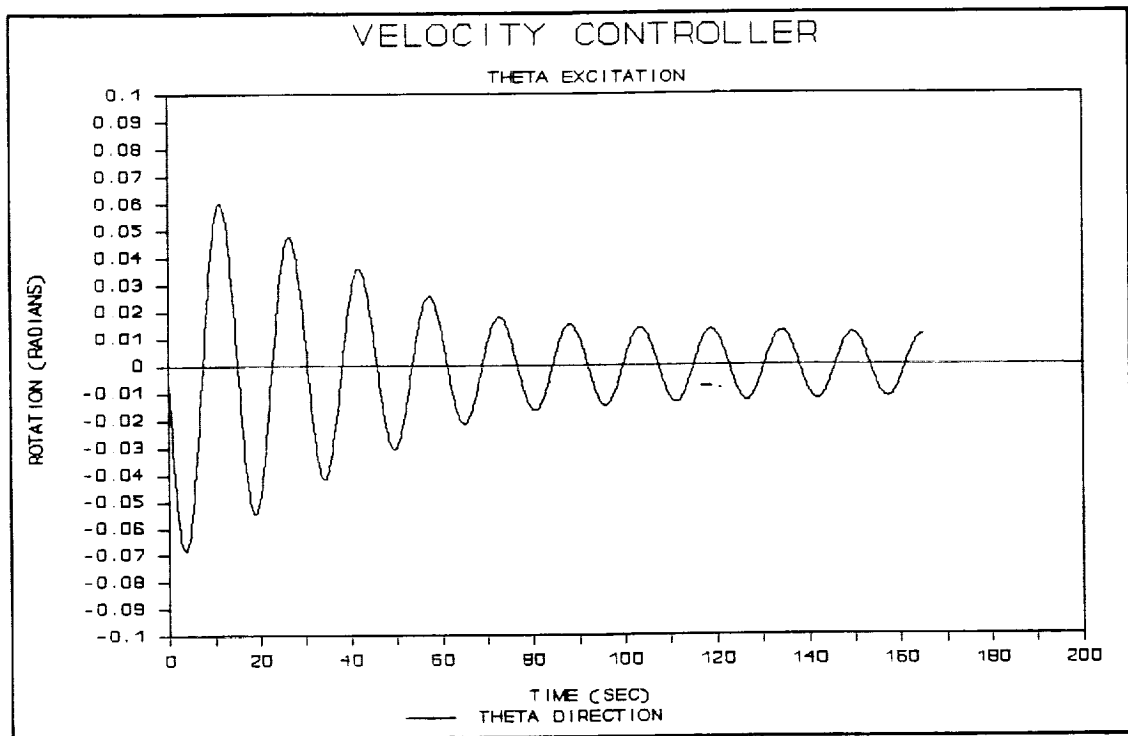


Figure 36 Experiment: Velocity Control,  $\theta$  IC,  $\theta$  Dir

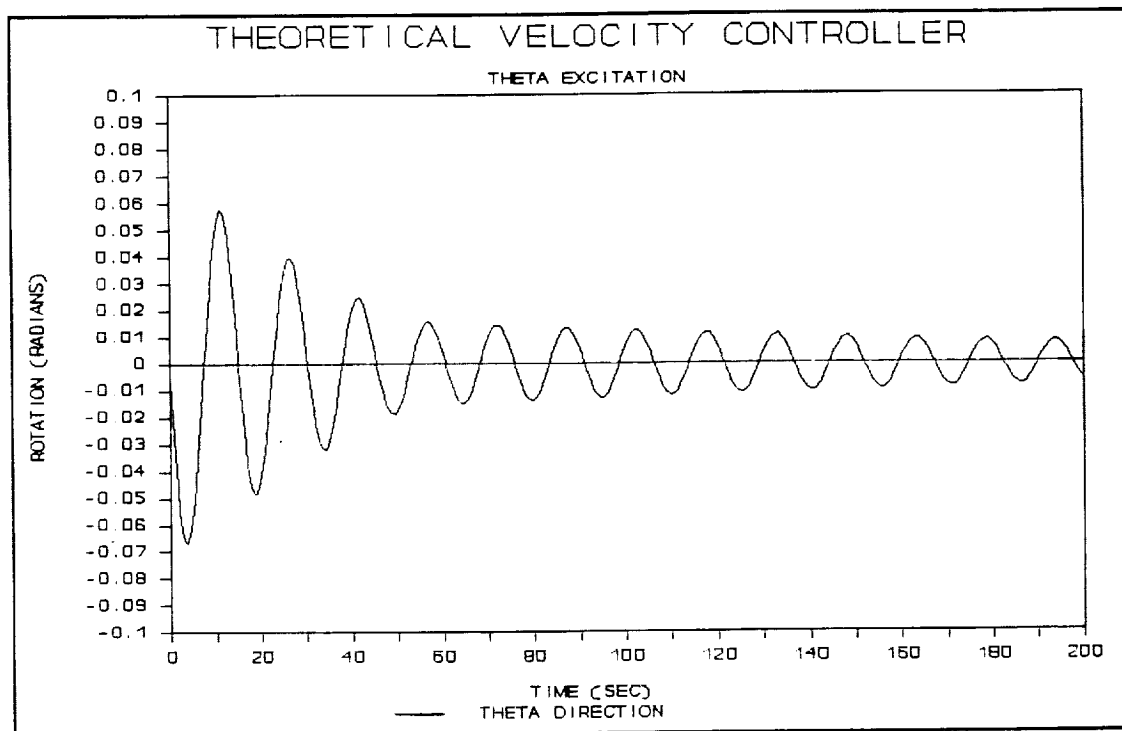


Figure 37 Theory: Velocity Control,  $\theta$  IC,  $\theta$  Dir

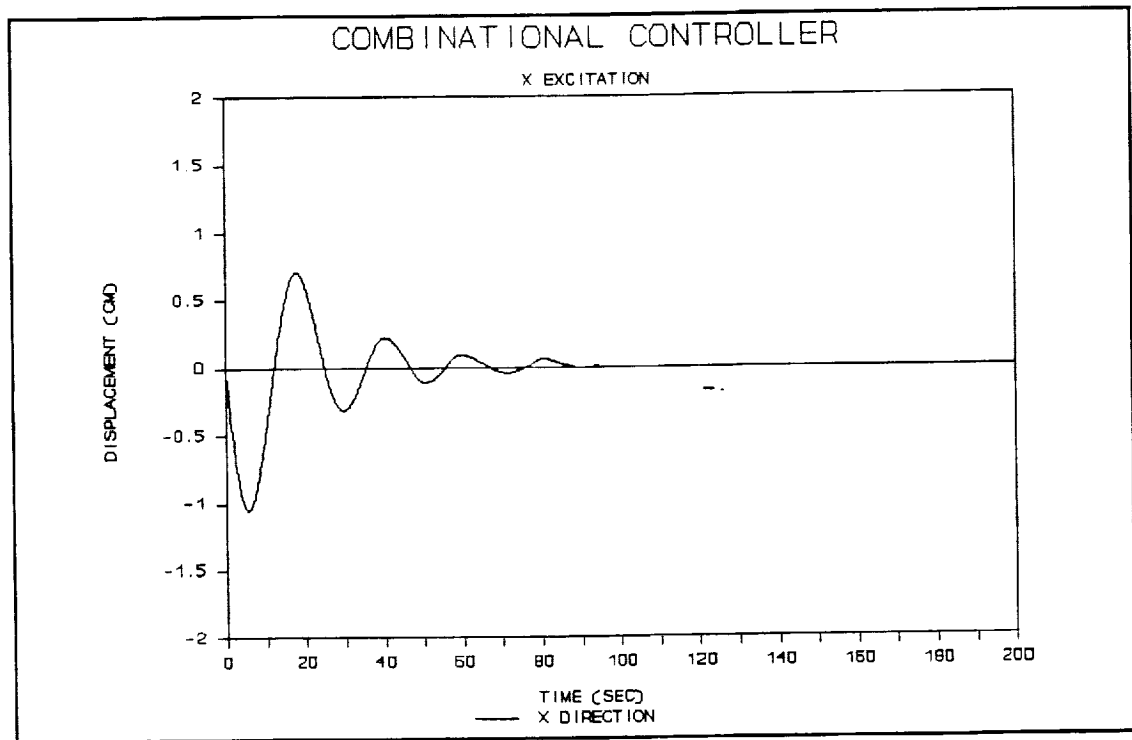


Figure 38 Experiment: Combinational Control, X IC, X Dir

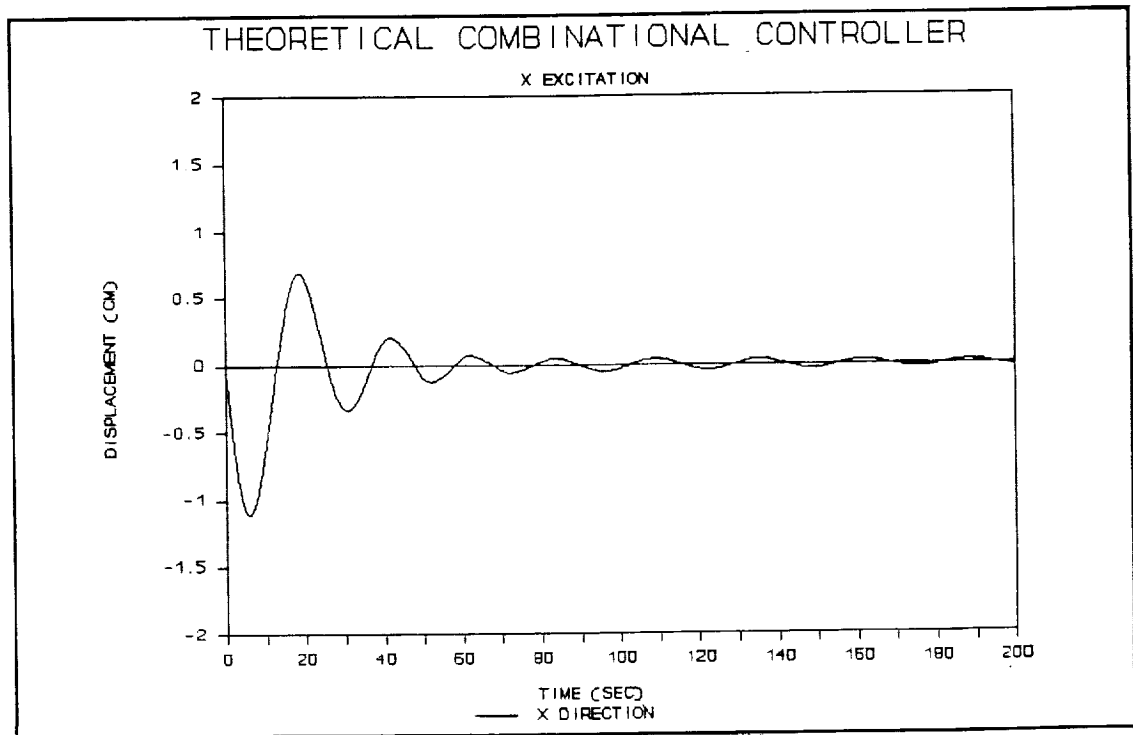


Figure 39 Theory: Combinational Control, X IC, X Dir

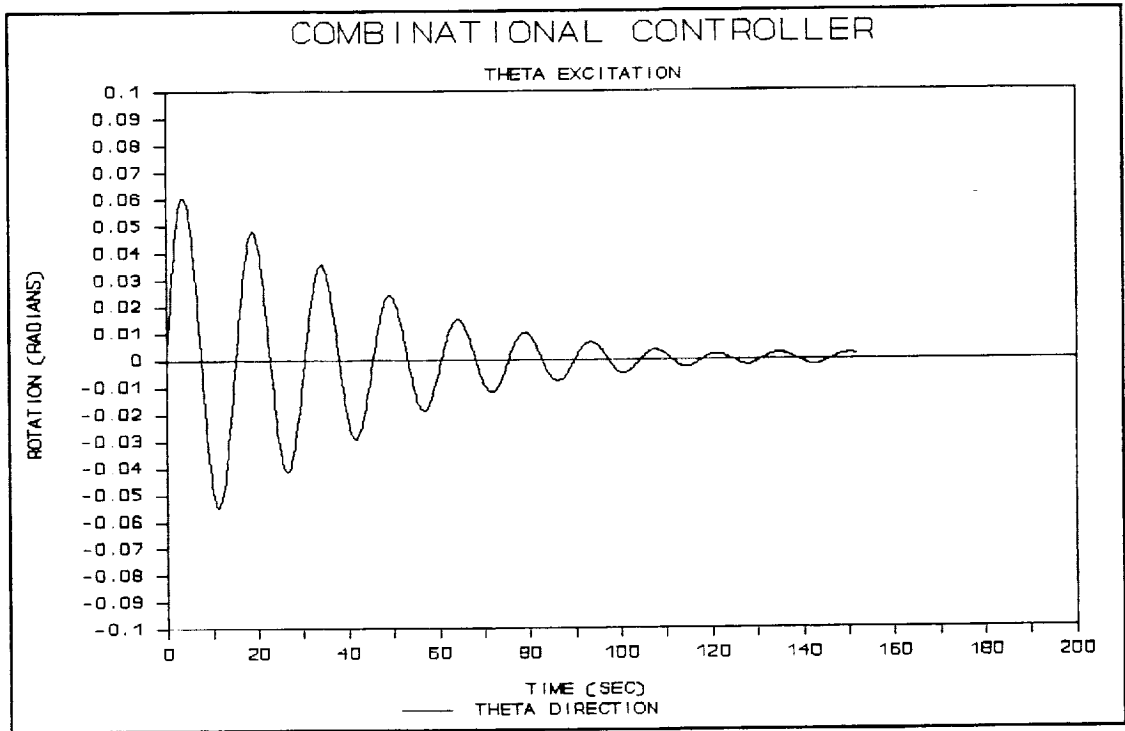


Figure 40 Experiment: Combinational Control,  $\theta$  IC,  $\theta$  Dir

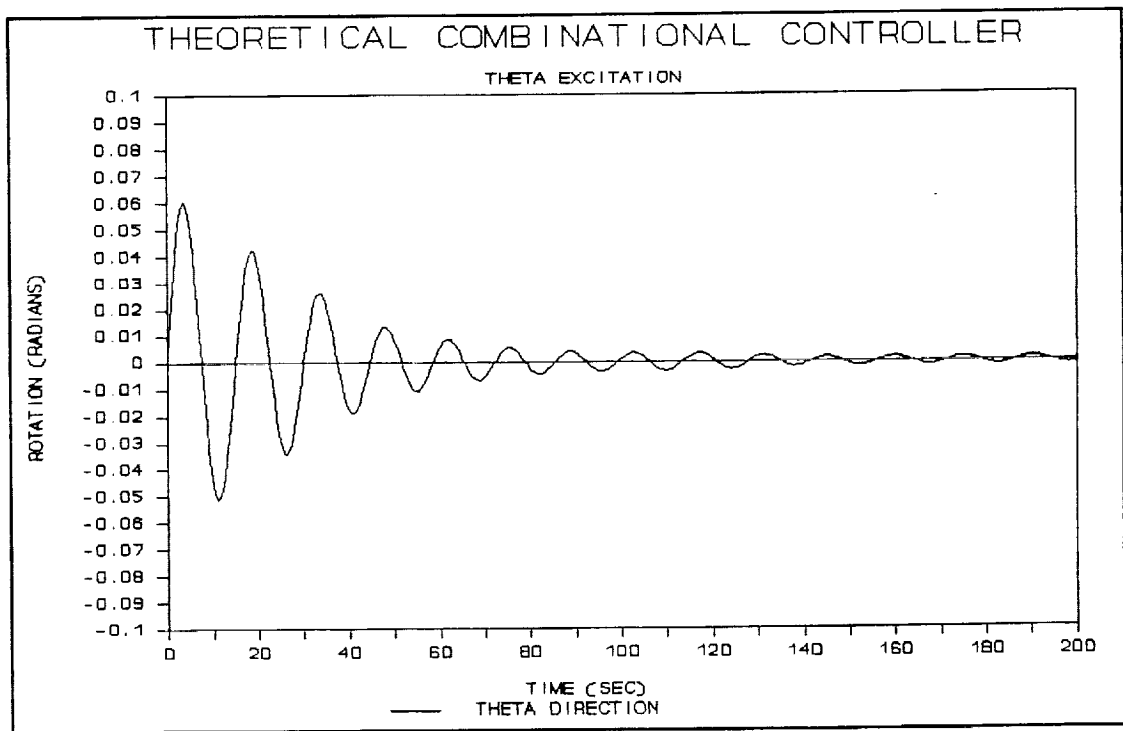


Figure 41 Theory: Combinational Control,  $\theta$  IC,  $\theta$  Dir

## Payload Response to Typical Disturbances

Payload response to two disturbances typical to the Space Station environment were investigated. The first was a 0.4g, 10 Hz harmonic excitation to the support structure (frame); the second a 350 micro-g acceleration pulse representing crew soaring activity. Since instrumentation for detecting payload acceleration in the micro-g range was not available, no experimental tests were conducted with these types of loads. Results presented here are analytical and are felt to be representative of response that would be experimentally observed.

### Harmonic excitation, no controller

It is useful to review the steady-state acceleration response of a single degree-of-freedom system with the excitation applied to the base, or frame. We are interested for now in response of the system without active control. The magnitude ratio is given as

$$\frac{a_o}{a_{in}} = \left[ \frac{1 + (2\zeta r)^2}{(1-r^2)^2 + (2\zeta r)^2} \right]^{1/2}$$

where

$a_o$  = payload acceleration

$a_{in}$  = excitation acceleration

$\zeta$  = damping ratio

$r$  = ratio of excitation frequency to system natural frequency  
(frequency ratio)

To achieve  $a_o \leq 10^{-5}g$  (the criterion used in this study) for  $a_{in} = 0.4g$ ,  $(a_o/a_{in}) \leq 2.5 \times 10^{-5}$ . This exceptionally high transmission loss requires the frequency ratio to be high, as shown in figure 42, a plot of the above equation for the region of interest here. Note in this case of unusually high frequency ratios that damping plays a dominant role in the isolation achieved.

For the experimental setup developed in this project the natural frequency in translation was 0.0382 Hz and the damping ratio was 0.017. Using these values ( $r=262$  for 10 Hz excitation) gives  $a_o = 5.2 \times 10^{-5}g$  for  $a_{in} = 0.4g$ , shown by the dotted lines on figure 42. The response is a factor of 5 higher than the desired value of  $10^{-5}g$ . The figure shows that the target acceleration level of  $(a_o/a_{in}) = 2.5 \times 10^{-5}$  can be obtained by increasing the frequency ratio, reducing the damping, or by a combination of the two.

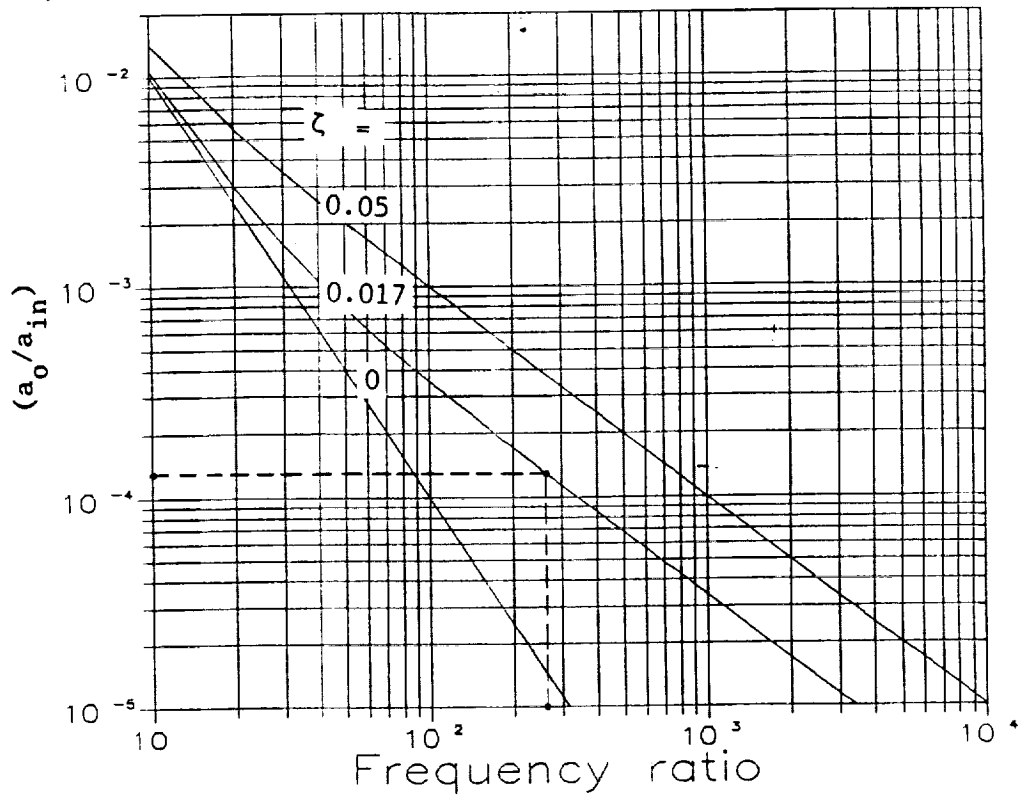


Figure 42 Harmonic Response Acceleration Magnitude Ratio

**Pulse excitation, no controller**

Consider the response of a single degree-of-freedom system to an acceleration pulse applied to the base, or frame. A single, 350 micro-g, one-second duration half-sine pulse is the input. The maximum response is (Harris and Crede, 1976):

$$\left( \frac{a_o}{a_{in}} \right)_{\max} = \frac{4(\tau/T) \cos \pi(\tau/T)}{1-4(\tau/T)^2}$$

where  $\tau$  = pulse duration  
 $T$  = system natural period

For the small values of damping considered here the peak response is independent of damping. In our problem,  $\tau = 1.0$  s,  $T = 26.2$  s, giving  $(a_o/a_{in}) = 0.153$ , so  $a_o = 5.36 \times 10^{-5}g$  for the 350 micro-g input. Again we note that the response is about a factor of 5 too high. In this case the peak acceleration can be reduced only by decreasing the ratio of pulse duration to system natural period.

## Harmonic excitation with controller

The computer model was used to predict behavior of the system when subjected to these typical disturbances with the air jet controller activated. The harmonic disturbance was modeled as a sinusoidal displacement to the frame of frequency 10 Hz and amplitude 1 mm (0.4g acceleration). Excitation was applied to the planar model in the Y direction. Simulation results with the combinational control show that the payload is excited not only from the disturbance but also from the jets firing. The combinational controller automatically turns on a solenoid when the velocity reaches a given threshold value. The sensor sees the relative displacement and velocity between the payload and itself. There may be situations in which the payload is not oscillating, but the structure on which the sensor is mounted is oscillating. The sensor reads the relative displacement and velocity and sends a signal to the computer that the payload is oscillating. Figure 43 shows the payload response to the harmonic excitation. The sharpness of the peaks is produced by the air jets. The air jet forces cause the acceleration to be about 40% higher than it would be without the controller on. This is due to the controller sensing the relative motion between the payload and the harmonically moving structure and hence causing the jets to fire in the direction to increase the acceleration.

For a harmonic amplitude of 1 mm the maximum velocity is 0.0628 m/s. This signal is passed through an analog filter, as described earlier, which attenuates frequencies greater than 1 Hz at a rate of 20 db/dec. The forcing frequency is one decade away from the cutoff frequency and is attenuated to 10% of its original value. This gives a maximum velocity, seen by the controller, of 0.00628 m/s. This number is higher than the velocity threshold value of 0.001 m/s, causing the jets to fire approximately 90% of the time. This behavior is unacceptable from a power consumption view point.

There are several ways to prevent unwanted jet firings, such as using a higher order filter to further attenuate the velocity signal, or increasing the velocity threshold value. If the threshold is increased sufficiently the combinational control reduces to displacement control. If displacement control is used, the jets are never fired in response to this harmonic disturbance. When the jets are not fired the amplitude of oscillation predicted by the computer model matches that determined in the "no controller" discussion on p. 48, as shown in figure 44.

Additional study is needed to determine the worst case excitation conditions and resulting payload response.

## Pulse excitation with controller

In order for the crew to move about, they must push off the side of the Space Station structure. This motion may be detected by the sensing unit of the control system or transmitted through utility connections to the payload. The soaring activity was

modeled as two half-sine wave acceleration pulses with a 350 micro-g amplitude. A positive pulse is followed, after a 3-second delay, by an equal but negative pulse. The second pulse is from the reactionary force when the crew member reaches another wall.

Figure 45 shows payload response in the Y-direction to a single half-sine pulse in that direction with the controller off. The peak acceleration agrees with the value determined in the "no controller" discussion on p.49. Figure 46 shows the response to the same input but with the displacement controller activated. The air jet forces cause the abrupt changes in acceleration. The combinational controller produced a similar response. Note that the controller damps the motion rather quickly, but the peak acceleration is higher than that obtained with no control. Again, this is due to the controller sensing the relative motion between the payload and sensors.

Figure 47 shows payload response to the two half-sine pulses with displacement control; results with combinational control are similar. It should be noted that the peak acceleration produced by the positive-negative pulse pair depends on the time between pulses compared to the natural period of oscillation of the system. This timing may subtract from or add to the response.

# ACCELERATION OF CENTER OF MASS

SINUSOIDAL INPUT; COMBINATIONAL CONTROL

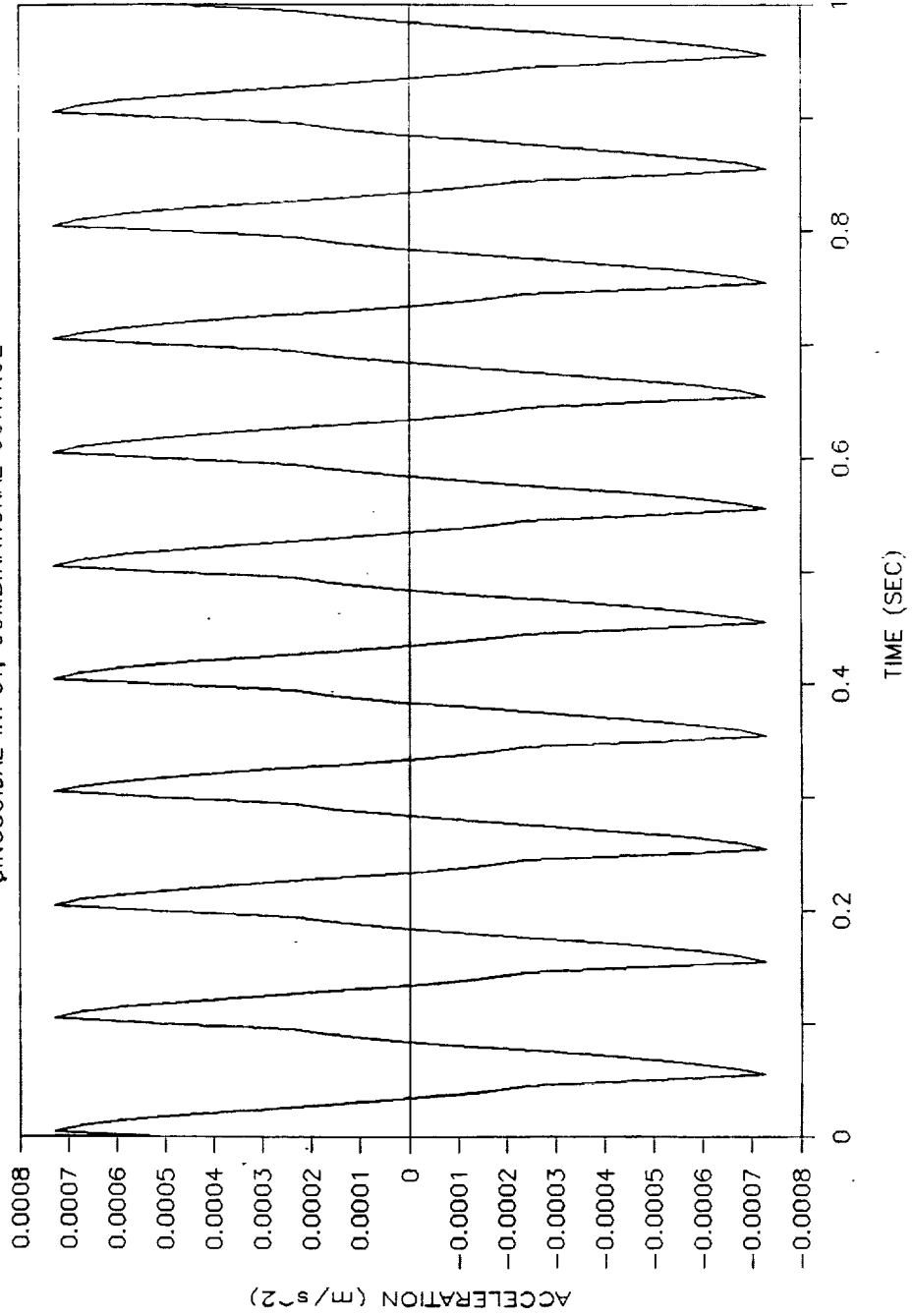


Figure 43 Payload Response to Harmonic Excitation with Combinational Control

# ACCELERATION OF CENTER OF MASS

SINUSOIDAL INPUT; DISPLACEMENT CONTROL

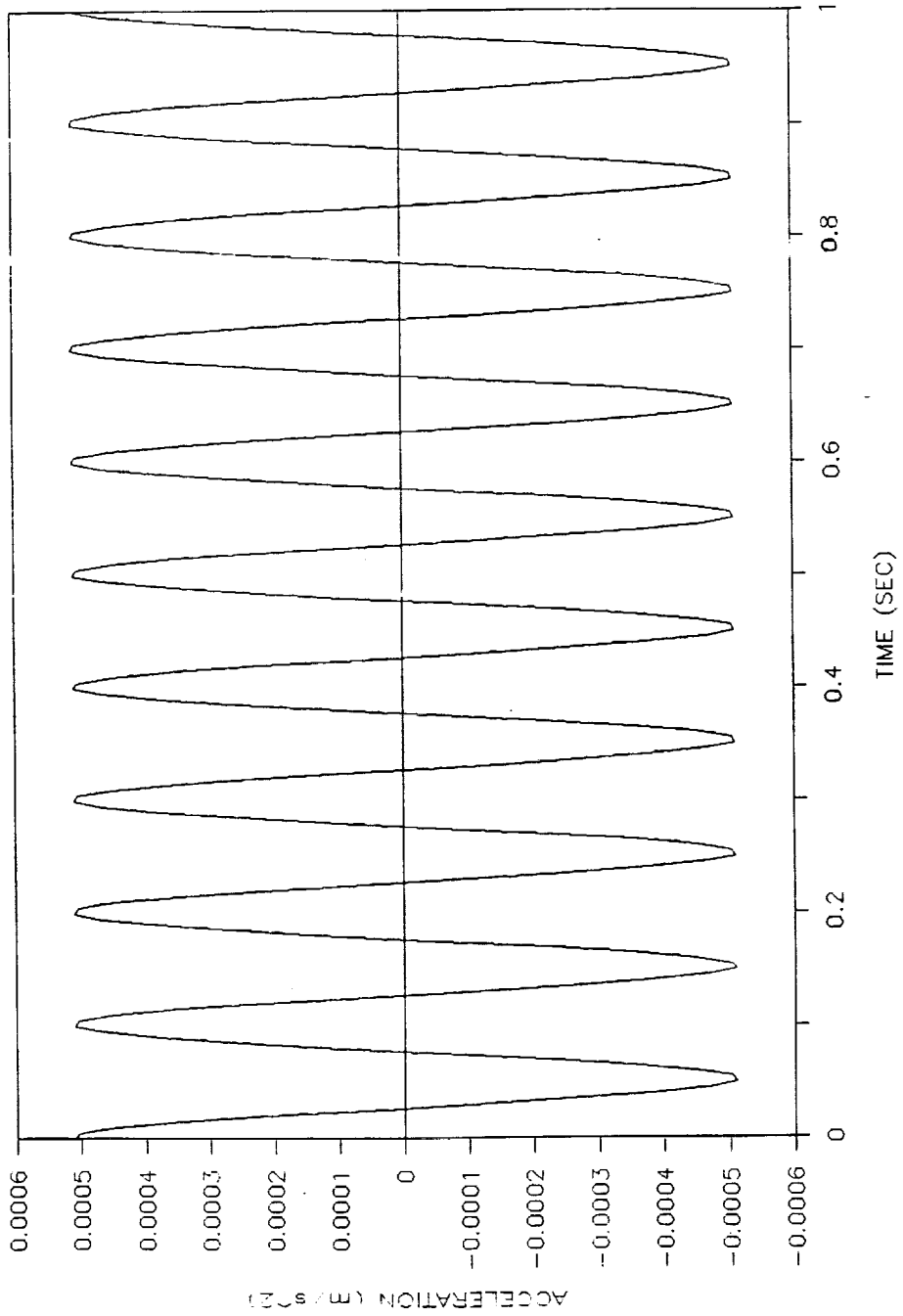


Figure 44 Payload Response to Harmonic Excitation with Displacement Control

# ACCELERATION OF CENTER OF MASS

1 IMPULSE INPUT; UNCONTROLLED

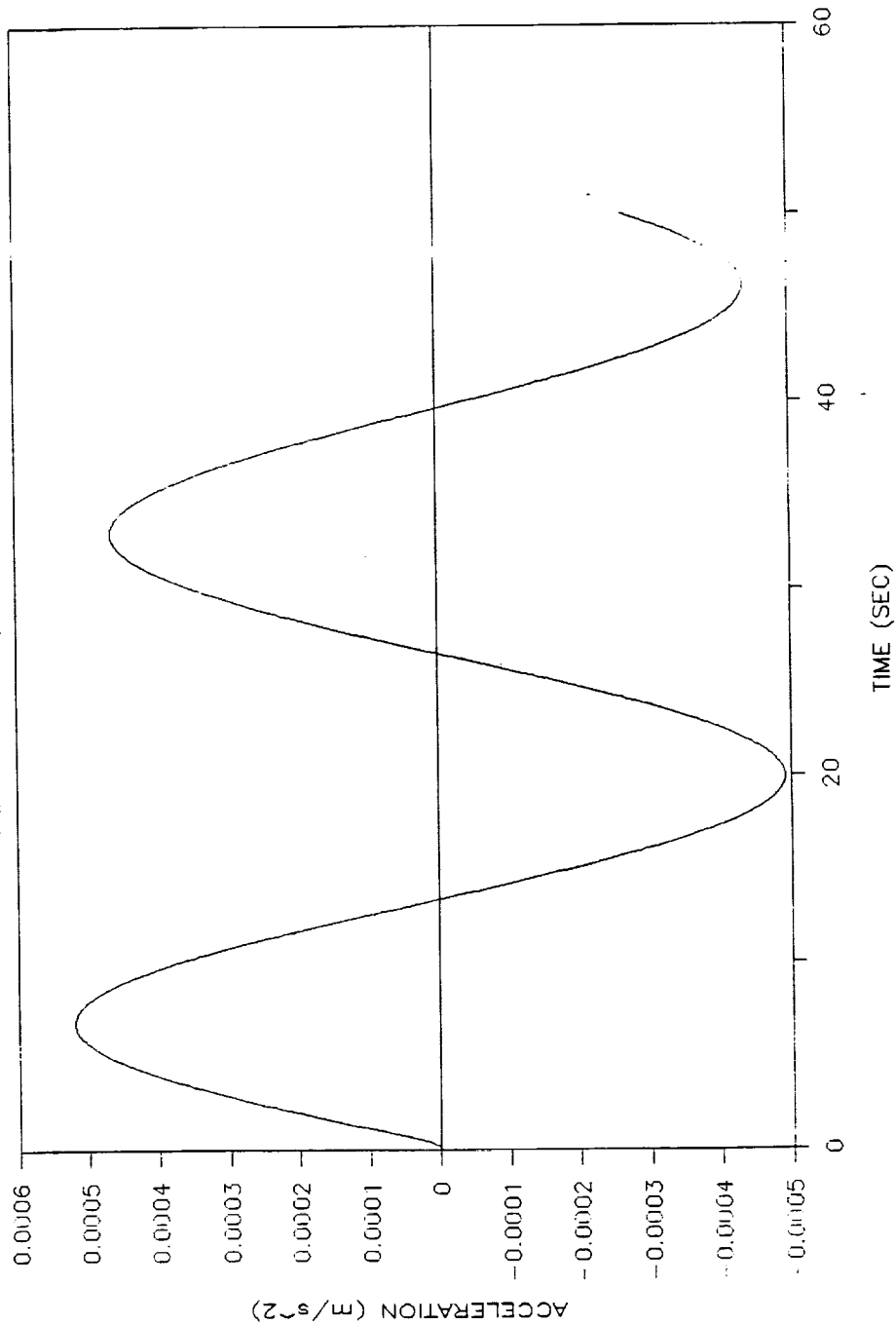


Figure 45 Uncontrolled Payload Response to a Single Half-sine Pulse

ORIGINAL PAGE IS  
OF POOR QUALITY

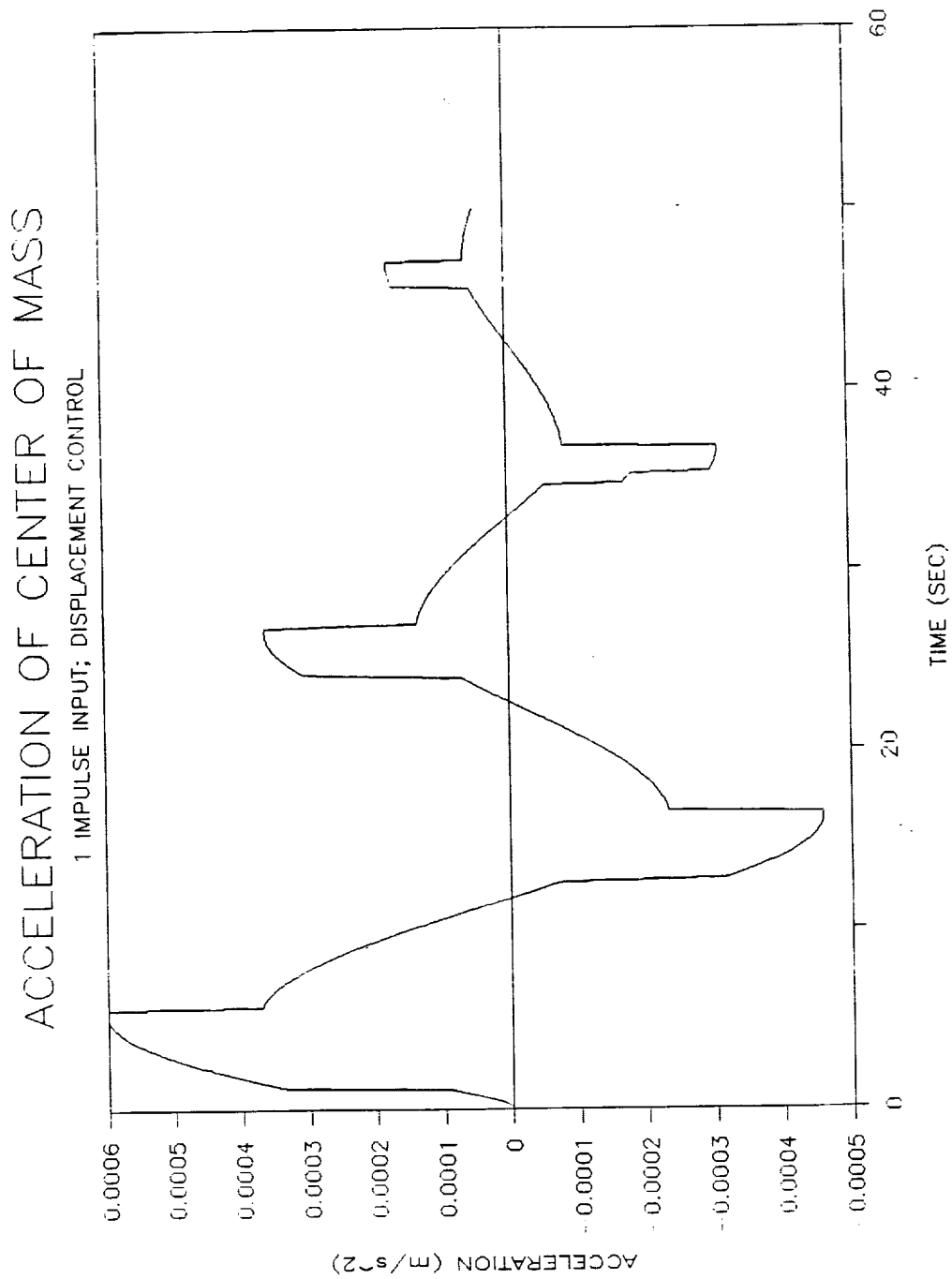


Figure 46 Payload Response to a Single Half-sine Pulse  
with Displacement Control

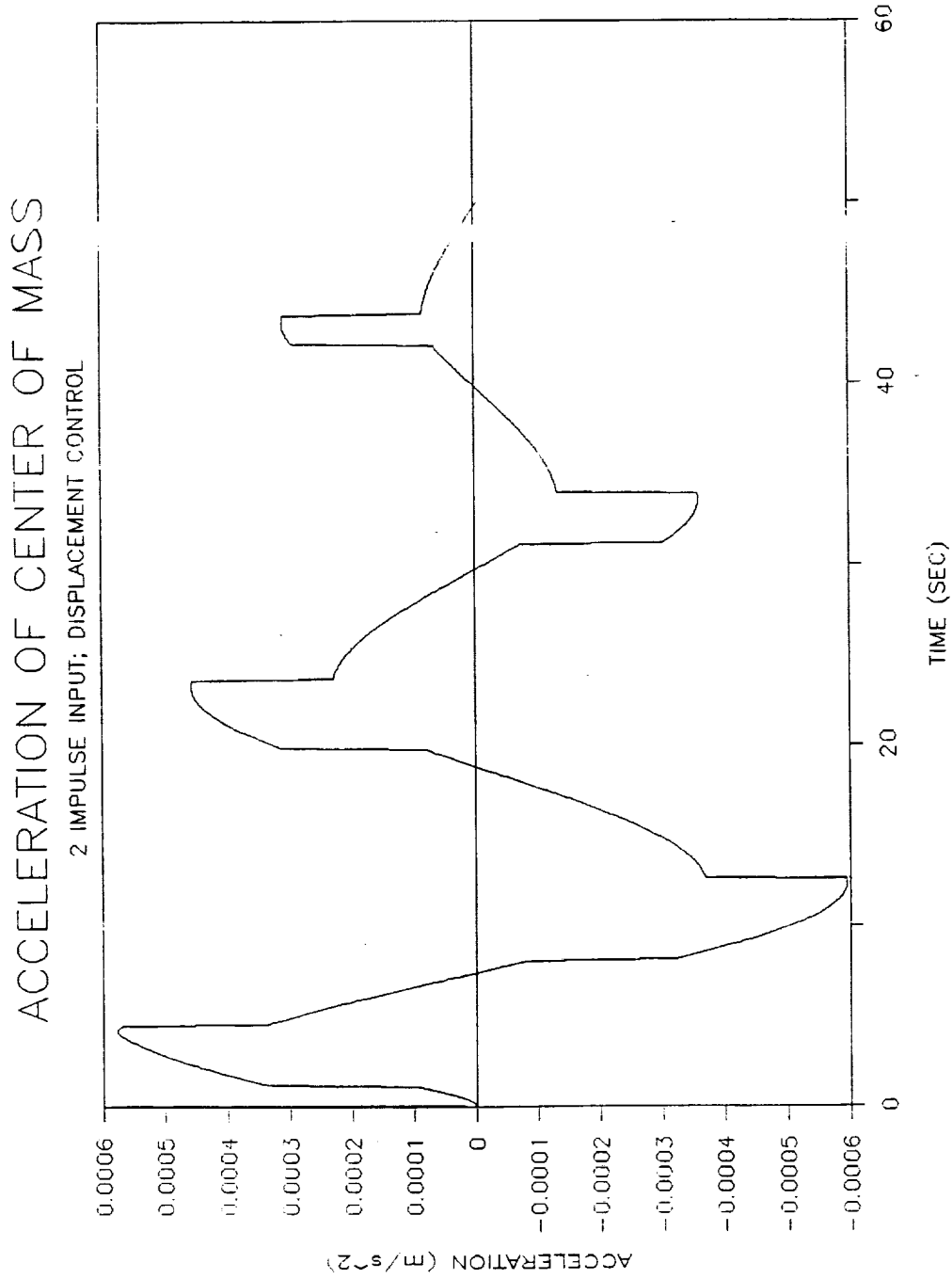


Figure 47 Payload Response to a Positive-Negative Pulse  
Pair with Displacement Control

## VI. LIMITATIONS

One of the objectives of this project was to develop an experimental setup to simulate the low-g environment of space. This has been accomplished through use of a low-friction air-bearing table with a payload, representing a scientific experiment package, moving in the horizontal plane. Although friction was minimized in the setup it is most likely higher than will be present in the actual space environment. As discussed on p. 48 of this report the magnitude of damping (friction) present greatly influences the degree of isolation achieved. For example, an accurate prediction of payload response to harmonic excitation requires a precise value of system damping. Results given in this report are based on the natural frequencies and damping of the experimental setup. Actual in-space payload response will differ from that reported here, due in part to the discrepancy between actual and modeled damping values.

This study dealt with two-dimensional payload motion. Results obtained are thus limited, since the actual payload will move in three dimensions. This limitation can be overcome by the development of a three-dimensional analytical model.

## VII. SUGGESTED ADDITIONAL EFFORT

1) The analytical simulation developed in this project should be utilized to predict payload response to the newly-defined dynamic excitations described in "Space Station Freedom, Microgravity Environment Definition, Study 3-01, NASA, Washington, D.C., February, 1989). Calculated response acceleration levels would then be compared to the revised criteria established in Study 3-01 to determine the feasibility of implementing the air jet control system.

2). Scientific experiments conducted in space will require isolation in three dimensions. The current project investigated planar isolation methodologies. The analytical simulation developed during this contract should be expanded to allow the study of three-dimensional payload motion. Revised and more complex logic will be required for three-dimensional payload motion control than for two-dimensional control. This additional effort is a prerequisite to the design and implementation of a flight-ready isolation system.

3). The experimental portion of this project was hampered by the lack of low-cost instrumentation to detect micro-g acceleration levels. The question of how to continuously monitor in-flight experiment vibration is an important one that must be addressed. An effort is required to develop such instrumentation for use on earth (in micro-g research and simulation) as well as in space.

## VIII. CONCLUDING REMARKS

An experimental and analytical study has been conducted to develop methods to isolate vibration-sensitive scientific experiments from dynamic excitations that will occur in the Space Station. A low-g simulator was designed and successfully implemented in the Shock and Vibration Laboratory at Texas A&M University. An analytical model was developed and verified by comparing predicted and experimental results. The mathematical model can now be employed to further investigate payload response to any type of disturbance and to examine controllers not yet developed.

This study has shown that the air jet controller successfully controls payload transient motion by removing energy from the motion, e.g., the controller actively damps the motion. The controller proved to be effective in centering the payload within a prescribed boundary. It should be emphasized that while the controller is effective in controlling low-frequency payload excursions, the passive portion of the vibration isolation system determines, for the most part, the peak payload acceleration to pulse and harmonic-type disturbances. Thus, if utility lines connect the Space Station structure to a scientific experiment, the spring rate of these lines must be extremely small. It is best, of course, to have no vibration transmission path from the structure to the experiment.

This project has laid the groundwork for developing an isolation scheme to be implemented in the Shuttle or Space Station. Additional work is necessary at this point to design a system to effectively isolate three-dimensional payload motion.

## REFERENCES

Atwood, Clay, May 1990, "Design and Analysis of Active Vibration Control in a Microgravity Environment", Master of Science Thesis, Mechanical Engineering Department, Texas A&M University, College Station, Texas.

Beckwith, T.G., Buck, N.L., and Marongoni, R.D., 1982, Mechanical Measurements, Addison-Wesley Publishing Co., Reading, Mass., pp. 483-512.

Cordera, Joseph C., May 1990, "Experimental Verification of Active Vibration Control in a Microgravity Environment", Master of Science Thesis, Mechanical Engineering Department, Texas A&M University, College Station, Texas.

Dodge, R.A. and Thompson, M.J., 1937, Introduction to Fluid Mechanics, McGraw-Hill Book Co., New York, NY, pp. 284-294.

Fox, R.W. and McDonald, A.T., 1985, Introduction to Fluid Mechanics, John Wiley & Sons, Inc., New York, NY, pp. 561-583.

Garriott, O.K. and DeBra, D.B., 1985, "A Simple Microgravity Table for the Orbiter or Space Station," Earth-Orientation Applications to Space Technology, NASA-Johnson Space Center, Vol. 5, No. 3, pp.161-163.

Gerhart, P.M. and Gross, R.J., 1985, Fundamentals of Fluid Mechanics, Addison-Wesley Publishing Co., Reading, Mass.

Gerhold, C.H. and Alexander, R.M., February 1987, "Microgravity Vibration Isolation - Design Criteria and Isolation Parameter Identification," TEES Project No. 21840, Texas Engineering Experiment Station, College Station, Texas.

Gerhold, C.H. and Rocha, R., 1988, "Active Vibration Control in Microgravity Environment," Journal of Vibration, Stress, and Reliability in Design, ASME, Vol. 110, pp.30-35.

Gilbride, J.F., 1983, "Modified Shielding Jet Model for Twin-Jet Shielding Analysis," Master of Science Thesis, Texas A&M University, College Station, Texas.

Harris C.M. and Crede, C.E., 1976, Shock and Vibration Handbook, Second Edition, McGraw-Hill, New York, NY, p. 8-48.

Jameson, A.H., 1942, Introduction to Fluid Mechanics, Longmans, Green and Co. Ltd., London, pp. 47-56.

Martin-Marietta, 1986, Report No. SSP-MMC-00019, Revision A, Section 2.0, "U.S. Laboratory Overview," Martin-Marietta Aerospace, Boulder, Colorado.

Mims, Forrest M. III, 1982, Engineer's Notebook II. A Handbook of Integrated Circuit Applications, Radio Shack, Dallas, Texas.

Park, M.S., 1987, "Active Vibration Control in a Microgravity Environment," Master of Science Thesis, Texas A&M University, College Station, Texas.

Space Station RUR-2 Data Package, End Item Data Book, Book 3 MTL Module, Contract NAS8-36525, DR No. 19, SSP-MMC-00012.

Steidel, Robert F., Jr., 1979, An Introduction to Mechanical Vibrations, Second Edition, John Wiley & Sons, Inc., New York, NY, p. 57.

Strum, Robert D. and Kirk, Donald E., 1988, First Principles of Discrete Systems and Digital Signal Processing, Addison-Wesley, New York, NY.

Thomson, W.T., 1988, Theory of Vibration with Applications, Prentice-Hall, Englewood Cliffs, New Jersey.

Wyle Laboratory, 1985, "Manufacturing & Technology Laboratory Customer Requirements Analysis," Research Report, EMS Product; MSFC-WP01: EMS R.1.4.

**DISTRIBUTION LIST**

NASA Lyndon B. Johnson Space Center  
Attn: Mail Code ES4 / Mr. R. Rocha  
Houston, TX 77058  
(2 copies)

NASA Lyndon B. Johnson Space Center  
Attn: Mail Code BE31 / Mr. J. Gips  
Houston, TX 77058  
(1 copy)

NASA Scientific and Technical Information Facility  
Attn: Accessioning Department  
P.O. Box 8757  
Baltimore/Washington International Airport, MD 21240  
(1 copy)

